Endonuclease Activity Inhibition of the NS1 Protein of Parvovirus B19 as a Novel Target for Antiviral Drug Development

Peng Xu[1], Safder S. Ganaie[1], Xiaomei Wang[1], Zekun Wang[1], Steve Kleiboeker[2], Nancy C. Horton[3], Richard F. Heier[4], Marvin J. Meyers[4,5], John E. Tavis[6], and Jianming Qiu[1]

[1]Department of Microbiology, Molecular Genetics and Immunology
University of Kansas Medical Center
Kansas City, KS 66160

[2]ViraCor Eurofins Laboratories
Lee's Summit, MO 64086

[3]Department of Molecular and Cellular Biology
University of Arizona
Tucson, AZ 85721

[4]Center for World Health and Medicine
[5]Department of Chemistry
[6]Department of Molecular Microbiology and Immunology
Saint Louis University
St. Louis, MO 63104

Running title: B19 NS1 endonuclease as a target for anti-B19 drugs

[#]Corresponding author:

Department of Microbiology,
Molecular Genetics and Immunology
University of Kansas Medical Center
Mail Stop 3029
3901 Rainbow Blvd.
Kansas City, KS 66160

Phone: (913) 588-4329
Fax: (913) 588-7295
E-mail: jqiu@kumc.edu

Version_11-15-18

ABSTRACT

Human parvovirus B19 (B19V), a member of the genus *Erythroparvovirus* of the family *Parvoviridae*, is a small non-enveloped virus that has a single-stranded DNA (ssDNA) genome of 5.6 kilobases with two inverted terminal repeats (ITRs). B19V infection often results in severe hematological disorders and fetal death in humans. B19V replication follows a model of rolling hairpin-dependent DNA replication, in which the large non-structural protein NS1 introduces a site-specific single strand nick in the viral DNA replication origins, which locate at the ITRs. NS1 executes endonuclease activity through the N-terminal origin binding domain. Nicking of the viral replication origin is a pivotal step in rolling hairpin-dependent viral DNA replication. Here, we developed a fluorophore-based *in vitro* nicking assay of the replication origin using the origin binding domain of the NS1 and compared it with the radioactive *in vitro* nicking assay. We used both assays to screen a set of small molecule compounds (96) that have potential anti-nuclease activity. We found that the fluorophore-based *in vitro* nicking assay demonstrate sensitivity and specificity values as high as the radioactive assay. Among the 96 compounds, we identified 8 which have an inhibition of >80% at 10 μM in both the fluorophore-based and radioactive *in vitro* nicking assays. We further tested 3 compounds that have flavonoid-like structure for IC_{50} *in vitro* that falls in the range of 1-3 μM. Importantly, they also exhibited inhibition of B19V DNA replication in UT7/Epo-S1 cells and *ex vivo* expanded human erythroid progenitor cells.

KEY WORDS: Human parvovirus B19**,** *in vitro* nicking assay, anti-viral compounds

Antimicrobial Agents and Chemotherapy

INTRODUCTION

Human parvovirus B19 (B19V) was identified in 1975 when Yvonne Cossart screened hepatitis B virus in a panel of human serum samples (1). B19V is a small, non-enveloped single-stranded DNA (ssDNA) virus belonging to the genus *Erythroparvovirus* within the family *Parvoviridae* (2). B19V exhibits a remarkable tropism for human erythroid progenitor cells (EPCs) in the bone marrow and fetal liver (3-7). B19V most commonly causes Fifth disease or slapped cheek syndrome in children (8,9); however, B19V infection can cause a series of severe hematological disorders (10). B19V infection of the fetus can cause severe fetal anemia, resulting in non-immune hydrops fetalis and fetal death (11-14). In certain circumstances, B19V infection often results in bone marrow failure, most notably transient aplastic crisis in patients with increased red blood cell turnover (e.g., sickle cell disease patients), and pure red-cell aplasia in immunodeficient and immunocompromised patients (e.g., HIV/AIDS patients and organ transplant recipients) (11,15). The clinical manifestations of B19V infection, as seen in *hydrops fetalis*, transient aplastic crisis, and pure red-cell aplasia, are due to direct cytotoxicity resulting from virus infection, which results in the death of EPCs in which B19V replicates (5,16-22).

B19V has a linear ssDNA genome of about 5.6 kilobases (kb), which has identical terminal repeats (ITRs) of 383 nucleotides at both ends. The double-stranded replicative form (RF) DNA of the B19V genome contains a P6 promoter at the left hand (10). The left side of the RF genome encodes a large non-structural protein (NS1) and a small non-structural protein 7.5-kDa protein, whereas the right side of the genome encodes two capsid proteins (VP1 and VP2), along with a small nonstructural protein 11-kDa using a different open reading frame (23). B19V NS1, 671 amino acids (aa) long, has a molecular weight of approximate 78 kDa (**Fig. 1A**) (24,25). NS1 predominantly localizes in the nucleus of infected cells as it contains nuclear localization signals at aa residues 177-180 (KKPR) and 316-321 (KKCGKK), respectively (25,26). The N-terminus (aa 1-176) of the NS1 contains a DNA replication origin-binding domain

104 (OBD) that also exhibits endonuclease activity (27,28); the central region contains ATPase and
105 nucleoside triphosphate binding motifs (20); and the C-terminus contains transactivation
106 domains (20,29). NS1 is essential for replication of viral DNA through its endonuclease and
107 helicase activities (30). NS1 also binds the P6 promoter of the viral RF genome to regulate viral
108 gene expression (31). In addition, NS1 has been reported to transactivate several other host
109 genes (29,32,33).

110 B19V is an autonomous parvovirus, replicating itself in the host cells without a helper
111 virus (10), as are the majority of the members in the *Parvoviridae* family except for adeno-
112 associated viruses (AAVs) (34). In contrast, AAVs, whose genome also contains their unique
113 ITRs of 144 nucleotides, requires coinfection of a helper virus, such as adenovirus, herpesvirus,
114 or human bocavirus, for replication (35,36). B19V replication arrests cell cycle at late S phase,
115 hijacks cellular DNA replication factors present in the S phase, and replicates its genome
116 following a rolling hairpin model of DNA replication (37-39). In principle, the B19V ssDNA
117 genome uses 3′-end hairpin as a self-primer (3'OH) to extend viral ssDNA into the dsDNA
118 genome by cellular replication proteins (40), a step called first-strand DNA synthesis (39). The
119 extended 3′ end is presumably ligated to the 5′ end of the genome to form a partial circular DNA
120 genome. NS1, which has site-specific endonuclease activity and DNA helicase activity, nicks
121 ssDNA at the terminal resolution site (trs) between the 5'-end hairpins and the newly
122 synthesized viral DNA to form a novel 3' primer that initiates hairpin transfer, followed by the
123 strand displacement (39). The elongated viral genomes (both RF and double RF intermediates)
124 are also resolved by NS1 nicking to release ssDNA that is finally packaged into the capsid.

125 The minimal replication origin (Ori) of B19V DNA has been identified to be 67-nt, which
126 includes a STAT5-binding element (STAT5BE), a trs or nicking site, two copies of NS1-binding
127 element (NS1BE), and the putative cellular factor-binding site (CFBE) (**Fig. 2A**) (25,27,41,42).
128 Specific cleavage of the ssDNA Ori has been demonstrated in an *in vitro* nicking assay using
129 purified B19V NS1 N-terminus (aa 1-176) and a 5' end [^{32}P] labelled oligo that contain the trs

(28). In this study, we further demonstrated the specificity of the radioactive nicking assay, and developed a non-radioactive nicking assay using an oligo of 20 nucleotides labelled with 6-carboxyfluorescein (FAM) and the quencher Iowa Black® FQ (IBFQ) at the 5' and 3' ends, respectively. The fluorophore-based nicking assay recapitulates the same sensitivity and specificity as found in the radioactive assay. We further validated the assay using a small library of 96 compounds, where 8 compounds inhibited NS1 nicking activity by over 80%, and out of which 3 compounds also inhibited viral DNA replication in B19V RF DNA-transfected UT7/Epo-S1 cells and B19V-infected $CD36^+$ EPCs.

RESULTS

Purified NS1N, but not the endonuclease motif mutant, cleaves B19V Ori ssDNA, and does not cleave the mutant minimal replication origin (Ori).

B19V NS1 has the endonuclease activity at the N terminus aa 1-176 (NS1N, **Fig. 1A**). NS1N has been proved to bind the Ori and executes its cleavage *in vitro* (27,28). We first tested the specific Ori cleavage of the NS1N. To this end, we expressed and purified both the wild-type NS1N and $NS1N^{mEndo}$ that has alanine substitutions in the endonuclease motif (residues 140-143) (20) (**Fig. 1A**). Purified NS1N and $NS1N^{mEndo}$, which contain a 6 x histidine tag at the C-terminus, show a purity of >90% (**Fig. 1B&C**). We used a short version of the B19V ssDNA form Ori, which is 30-nt, as a template for cleavage, because the NS1-binding elements (NS1BEs) are not required for nicking of the ssDNA Ori in the condition of the *in vitro* nicking assay that contains high concentrations of NS1N (28). Ori30 and $Ori30^{mut}$ (**Fig. 2A**) were 5' end labeled with ^{32}P and then used at a final concentration of 2 nM in the nicking buffer (see **MATERIALS AND METHODS**) with 2 μM of the purified NS1N. After incubation of 16-18 h at 37°C, the reactions were analyzed in a denaturing urea polyacrylamide gel. We found that NS1N cleaved Ori30 at the trs and produced a cleaved DNA band at 19-nt (**Fig. 2B**, lane 4), while NS1N did not cleave the trs mutant $Ori30^{mut}$ (**Fig. 2B**, lane 5). Moreover, we asked whether the NS1N nick

Antimicrobial Agents and Chemotherapy

is endonuclease motif-specific. We used the purified NS1N^{mEndo} in the nicking assay. The result showed that while the wild-type NS1N was capable of cleaving the Ori-30 at trs and released a band of 19-nt, the NS1N^{mEndo} did not (**Fig. 2C**, lanes 3&4). We next determined the minimal concentration of NS1N required for nicking of the Ori. We found there was a dose-dependent increase in the level of the nicked band (19-nt) (**Fig. 2D**). At 2 μM of the NS1N, greater than 70% of the probe was cleaved. We chose to use NS1N at 2 μM in subsequent experiments.

Taken together, these results confirmed NS1N specifically and effectively cleaves the Ori (at 2 nM) at trs at a concentration as low as 2 μM, and that the endonuclease motif is important for the nicking activity.

Small molecule compounds inhibit cleavage of the ssDNA Ori by NS1N.

To identify small molecule compounds that can inhibit the NS1N-mediated Ori cleavage, we used 96 compounds (**Table S1 in Supplemental Materials**), which we have used previously to screen inhibitors for RNase H nuclease activity of the human hepatitis B (HBV) polymerase (43-47), to test them for inhibitory effects on the NS1N-mediated Ori cleavage using ^{32}P-labeled Ori30 template. We first tested them at 100 μM, and found that 25 compounds inhibited the nicking of NS1N by greater than 80% as shown in **Fig. 3A**. Next, we tested the positive 25 compounds at 10 μM. Eight compounds (#7, #9, #12; #135, #151, #153, #201, and #328) appeared to nearly abolish cleavage of the Ori by NS1N, a >80% inhibition compared with the DMSO control (**Fig. 3B**).

Fluorophore FAM-based nicking assay reproduces the sensitivity and specificity of the radioactive nicking assay.

We next developed a method that could screen a large number of compounds easily. We synthetized one fluorescent Ori oligo: ^{FAM}Ori20^{Q}, a 20-nt ssDNA oligo, in which the 5' end is labeled with FAM and the 3' end is labeled with a quencher IBFQ (**Fig. 4A**). The quencher dye

quenches the fluorescence emitted by the fluorophore via Förster resonance energy transfer (FRET) when the two dyes are in close proximity, and the intact $^{FAM}Ori20^{Q}$ did not show significant fluorescence. When NS1N was added, cleavage occurred at the trs, which resulted in an increase in fluorescence to a level of 72% of the fluorescence from the same oligomer but without a quencher present ($^{FAM}Ori20$), and the fluorescence intensity difference with or without NS1N reached 18.38-fold (**Fig. 4B**). We further tested the optimal concentration of the oligo. We found that at 25 to 200 nM of $^{FAM}Ori20^{Q}$, the assay displayed >20-fold difference in the fluorescence intensity with and without NS1N (**Fig. 4C**). Therefore, we chose $^{FAM}Ori20^{Q}$ at 200 nM in subsequent experiments based on the high fold change (20-fold) and the maximum fluorescence intensity (reading). We noticed that 2 μM of NS1N was enough to saturate the nicking of the Ori at concentrations ranging from 25 to 800 nM as increased fluorescence intensities were detected (**Fig. 4C**).

We next used the $^{FAM}Ori20^{Q}$ probe to repeat screening the 71 compounds (at 10 μM) which did not show >80% inhibition at 100 μM by the radioactive assay (**Fig. 3A**). We set up a cutoff value of 80% inhibition as in the radioactive assay, compared with the DMSO control. We found none of the 71 compounds showed an inhibition of >80% at 10 μM (**Fig. 5A**). We next carefully tested the 25 compounds, which showed an inhibition of >80% at 100 μM in the radioactive assay (**Fig. 3B**), at 10 μM with FAM-based nicking assay using $^{FAM}Ori20^{Q}$ probe. We found that 8 compounds (#7, 9, 12, 135, 151, 153, 201, and 328) were positive (>80% inhibition) in the inhibition of NS1N nicking activity (**Fig. 5B**). The results confirmed that the fluorescent assay detected all the 8 positive compounds from the radioactive assay.

We established the correlation coefficient value (r) between the two assays, which is 0.91 (**Fig. 5B**), indicating the two methods match well. We also generated the scatter plot and trendline of the two assays (**Fig. 5C**). The coefficient R squared value (R^2) is 0.83, representing smaller differences between the two assays.

207 Cheminformatics analysis showed that compounds #7, #9, #135, #201, and #328 have
208 flavonoid structures, while compounds #12, #151, and #153 possess naphthyridinone structures
209 (**Fig. 6**). We chose flavonoids compounds #7, #135, and #201 for further in-cell study below.
210
211 **Flavonoid compounds inhibit B19V DNA replication in UT7/Epo-S1 cells.**
212 We first determined the IC_{50} (the half inhibition of *in vitro* nicking) of the three flavonoids
213 compounds #7, #135, and #201, which are 3.1±0.8 μM, 2.9±0.8 μM, and 1.1±0.4 μM,
214 respectively (**Fig. 7**). We next asked whether they inhibited B19V DNA replication in B19V-
215 permissive cells. For a direct result of inhibition of viral DNA replication, we tested them in
216 UT7/Epo-S1 electroporated with a RF DNA of the B19V genome, the B19V infectious M20 DNA
217 (48). B19V infects UT7/Epo-S1 cells poorly (41,49) and electroporation using the nucleofector
218 (Lonza) directly delivers the viral double-stranded RF DNA into the nucleus, where the RF DNA
219 is nicked by NS1 to initiate viral DNA replication (39). After electroporation of the cells with
220 linearized M20 DNA, a compound was added at various concentrations. At two days post-
221 electroporation under hypoxic conditions, cells were collected for flow cytometry using an anti-
222 B19V capsid antibody to select capsid-expressing cells.
223 The half maximal effective concentration (EC_{50}) of B19V replication inhibition was
224 calculated compared with the vehicle control (DMSO). Compounds #7, #135, and #201 have
225 EC_{50} values of 44.2±18.6 μM, 61.1±0.3 μM, and 55.1±7.9 μM, respectively (**Fig. 8A**). The CC_{50}
226 (drug concentration that affects viability of 50% of cells in culture) values of compounds #7,
227 #135, and #201 as determined in UT7/Epo-S1 cells are 194.0±22.3 μM, 227.0±21.0 μM, and
228 180.9±20.5 μM, respectively (**Fig. 8B**). Therefore, the selective index ($SI=CC_{50}/EC_{50}$) for
229 compounds #7, #135, and #201 is 4.4, 3.7, and 3.3, respectively.
230 We further analyzed viral DNA replication in UT7/Epo-S1 cells using Southern blotting.
231 The results showed that at the concentrations close to their EC_{50}, compounds #7, #135, and

#201 inhibited at least half of the level of the RF DNA **(Fig. 9**). These results suggested that the inhibition of B19V replication is likely due to the inhibition of viral DNA replication.

Flavonoid compounds inhibit B19V infection in CD36$^+$ EPCs.

To mimic the B19V infection in human bone marrow, we used *ex vivo* expanded primary CD36$^+$ EPCs cultured under hypoxic conditions which were differentiated from CD34$^+$ hematopoietic stem cells isolated from human bone marrow. We infected the CD36$^+$ EPCs with B19V plasma, and at the same time, the cells were treated with various concentrations of the compounds. At 48 h post-infection, the cells were collected for determining B19V infection by flow cytometry using an anti-capsid antibody. We found that for compounds #7, #135, and #201, the EC_{50} is 37.6±3.6, 53.9±7.1, and 33.5 ±1.4 μM, respectively (**Fig. 10A**); the CC_{50} is 55.9±2.1, 89.8±7.8, and 60.0±2.4 μM, respectively (**Fig. 10B**). Therefore, the SI for compounds #7, #135, and #201 is 1.5, 1.7, and 1.8, respectively. For compound #7 at 40 μM, there were >95% living cells, whereas B19V infection was inhibited at an efficiency of >60%. For compound #135, at 50 μM, there were >95% living cells, whereas B19V infection was inhibited at an efficiency of 50%. For compound #201, at 40 μM, there were >80% living cells, whereas B19V infection was inhibited at an efficiency of 70% (**Fig. 10**). We next analyzed viral DNA replication in drug-treated infected cells at 48 h post-infection using Southern blotting. It was obvious that compounds #7, #135, and #201 inhibited viral DNA replication by over 10-fold at a concentration of 40, 50, and 50 μM, respectively (**Fig. 11**).

Furthermore, using quantitative PCR (qPCR), we were able to determine the inhibition of viral DNA replication by the compounds at early time (18 h) post-infection, compared to that at middle (30 h) and late times (48 h) during infection, respectively. At 18 h, 30 h and 48 h post-infection, cells were collected for extraction of total DNA which was subjected to qPCR for copies of viral genome relative to mitochondrial (mt) DNA, which was used to calculate EC_{50}. Compound #7 has EC_{50} values of 6.43±0.12 μM, 20.84±0.88 μM and 20.5±3.17 μM at 18 h, 30

h and 48 h post-infection, respectively (**Fig. 12A**); compound #135 has EC_{50} values of 20.47±1.11 μM, 31.28±1.95 μM and 38.35±4.68 μM at 18 h, 30 h and 48 h post-infection, respectively (**Fig. 12B**); and compound #201 has EC_{50} values of 20.47±1.11 μM, 16.15±0.54 μM and 24.51±0.1μM at 18 h, 30 h and 48 h post-infection, respectively (**Fig. 12C**). These results suggest all the three compounds showed a similar level of inhibition on the B19V DNA replication during early infection as effective as during middle and late time points of infection. Of note, compound #7 has a relatively effective EC_{50} of 6.4 μM at 18 h post-infection. Therefore, the selective indexes for compounds #7, #135, and #201 as determined by quantification of viral DNA at 48 h post-infection are 2.7, 2.4, and 2.5, respectively.

Collectively, these results demonstrated that compounds #7, #135, and #201 inhibited B19V infection and DNA replication in $CD36^+$ EPCs at a concentration that does not significantly kill cells.

DISCUSSION

In B19V infection-caused transient aplastic crisis, pure red-cell aplasia, chronic anemia and hydrops fetalis, the clinical manifestations are due to the direct cytotoxicity of the virus infection (11,15,21), a direct outcome of the cell cycle arrest and cell death of human erythroid progenitor cells (EPCs) that host B19V replication (5,16,18,19). To date, a vaccine against B19V infection and specific treatments for B19V infection-caused transient aplastic crisis, chronic anemia and pure red-cell aplasia, hydrops fetalis and congenital anemia in infants are not available. Although intravenous immunoglobulin (IVIG) can be administrated to patients with B19V-associated chronic anemia and pure red-cell aplasia (50-52), the symptoms often recur when IVIG treatment is interrupted (53-56). The repeated applications of IVIG and the maintenance therapy that are required to fully eliminate B19V-associated pure red-cell aplasia are cost prohibitive (51,57-63). As all these complications of hematological disorders caused by B19V infection are the direct outcome of B19V infection of EPCs, diminishing B19V replication

284 in EPCs is expected to be an effective approach for treating B19V infection-induced
285 hematological disorders. Cidofovir, an acyclic nucleoside phosphonate broadly against dsDNA
286 viruses, has shown some promises in antiviral effect on B19V infection (64,65). Small molecule
287 compounds that can specifically inhibit B19V replication of *ex vivo* expanded $CD36^+$ EPCs will
288 be ideal candidates to test as drugs for the treatment of hematological disorders caused by
289 B19V infection.

290 In the current study, we identified eight compounds that exhibit inhibition of NS1 nicking
291 of the B19V Ori from screening of 96 small molecule compounds, which have been used to
292 screen inhibitors for RNase H nuclease activity of the HBV polymerase (43-47), using an *in vitro*
293 nicking assay. We chose three compounds #7, #135, and #201, that share a flavonoid similar
294 chemo structure for detailed study. All three flavonoid compounds inhibited B19V DNA
295 replication in UT7/Epo-S1 cells and exhibited a selective index of 3-4. However, the compounds
296 showed higher cytotoxicity in primary $CD36^+$ EPCs with a therapeutic index of >1.5, although
297 they inhibited B19V infection at concentrations without showing significant cytotoxicity. These
298 data indicate that the 8 screening hits identified here are candidates for future medicinal
299 chemistry campaigns to improve efficacy and reduce cytotoxicity.

300 Flavonoids are a class of ubiquitous secondary plant metabolites. They have been
301 reported to have functions in a wide range of biological activity, including anti-microbe,
302 antioxidant, anti-cancer, anti-inflammatory and eukaryotic enzyme inhibition properties (66,67).
303 As antivirals, flavonoids been shown to execute antiviral activities against many human viruses,
304 including DNA viruses, RNA viruses, and retroviruses, observed in cell culture and animals (68).
305 Mechanistically, flavonoids function in various pathways of virus life cycle, including virus entry
306 (69), RNA transcription of viral genome (70,71), and viral RNA translation (72,73). Flavonoids
307 can inhibit viral protease activity (74,75), viral helicase activity (76,77), and viral (HIV) reverse
308 transcriptase (78,79). They also have been shown to suppress cellular pathway that are
309 essential to virus replication (80). Our studies expand the range of antiviral mechanisms

possessed by the flavonoids to include endonuclease activity of viral proteins (68). Flavonoids inhibited B19V infection, assessed for viral capsid expression, and B19V DNA replication in UT7/Epo-S1 cells nucleofected with M20 B19V infectious DNA (**Figs. 8&9**), as well as for B19V DNA replication during early infection of $CD36^{+}$ EPCs (**Fig. 12**), suggesting that the inhibitions likely take place in steps of viral DNA replication. As the nicking of the Ori by NS1 is an essential step for B19V DNA replication (81), we believe that flavonoids specifically target the nicking step. Another important class of small molecules that inhibits NS1N nicking is napthyridinone. Compounds #12 and #153 have been shown to inhibit the RNase H activity of the HBV polymerase (45,82). Naphthyridinones also have been shown to inhibit nuclease activity of the HIV reverse transcriptase (83). As a next step, we will test compounds #12, #151, and #153 for their activity against B19V infection in cells.

Identification of multiple hits in two chemotypes provides clues regarding the structure-activity relationships of these compounds. All of the flavonoid and napthyridinone hits share a hydrophilic two-ring heteroatom aromatic structure with a single appendage containing one or more benzyl moieties extending from similar spots on the bi-ring structure. Converting the benzylic extensions seen in the naphthyridinones #151 and #153 to a hydroxyl in #152 and #148 (**Fig. 6**) ablated activity against NS1N activity (**Figs. 3&5**). Similarly, ablating the hydroxyl on the nitrogen heteroatom in #12 to create #150 (**Fig. 6**) also ablated activity, possibly by removing the potential for chelation of the Mg^{++} ions in the NS1N active site that is known to be important as the naphthyridinones bind in this way against the HIV RNase H (84). These similarities will be valuable during future medicinal chemistry optimization of both the flavonoid and napthyridinone scaffolds.

An important contribution of this study is the establishment of a fluorescent *in vitro* nicking assay. We have identified the 67-nt Ori that supports B19V DNA replication in B19V-permisive UT7/Epo-S1 cells (41) and characterized the NS1BEs of the Ori *in vitro* (27). Based on this information, an *in vitro* nicking assay using a ^{32}P-labelled DNA probe, which spans the

trs in Ori, and purified B19V NS1N, was established (28). This radioactive nicking assay is not appropriate for high throughput screening of small molecule compounds that inhibit the B19V NS1N-driven nicking of the Ori. The NS1N cleaves ^{FAM}Ori20^{Q} probe efficiently and releases a significant fluorescent signal. Compared with the non-NS1N control, NS1N increases the fluorescence intensity by >18-fold, reaching ~72% of the signal from a non-quenched probe ^{FAM}Ori20. Notably, the FAM-based nicking assay possesses the same sensitivity and specificity in detecting inhibition of NS1N cleavage of the Ori as the radioactive nicking assay. The two assays exhibit a good correlation and minimal difference in detection of the NS1N-effected nicking of the B19V Ori. We expect this FAM-based fluorescent nicking assay could be utilized in high-throughput screening of large libraries of small molecule compounds for anti-B19V drug candidates.

MATERIALS AND METHODS

Compounds.

Compounds used in this study were as follows: #1-5, #7, #9-12, #19, #20, #23, #34 #49-52, #54, #60, #62, #64, #65, #67-69, #121, #125-130, #132, #134-139, #148-158, #197, #198, #200-209, #214, #215, #217, #218, #304, #307, #321-329, #338-346, #348-350, #352-357. Their structures are shown in **Table S1**. They were acquired commercially or synthesized (described in the **Supplemental Materials**) (85-87). Synthesized compounds were purified ≥95% purity as analyzed by HPLC. All compounds were dissolved in DMSO (Sigma, St. Louis, MO) and stored at -80°C.

Ethics statement.

Primary human CD34^{+} hematopoietic stem cells (HSCs) were isolated from bone marrow of a healthy human donor. We purchased them from AllCells LLC. (www.allcells.com, Alameda, CA), and obtained B19V-containng plasma samples from ViraCor Eurofins

Laboratories (Lee's Summit, MO). Both the cell and virus samples were deidentified, and therefore institutional review board (IRB) reviews were waived.

Cell line and primary cells.

Primary human CD36$^+$ erythroid progenitor cells (CD36$^+$ EPCs) (49,88): We *ex vivo* expanded CD34$^+$ hematopoietic stem cells under normoxic conditions (21% O_2; 5% CO_2) at 37°C until Day 4 (the day of procurement was designated Day 0). On Day 4, the expanded cells were frozen in liquid nitrogen as "Day 4 cells". For each experiment, Day 4 cells were thawed and cultured for 2 to 3 days in Wong expansion medium under normoxic conditions. On Day 6 or 7, the cells were cultured under hypoxic conditions (1% O_2 and 5% CO_2) for 2 days; these cells expressed CD36$^+$ (a marker for erythroid cells), and so we named them CD36$^+$ erythroid progenitor cells (CD36$^+$ EPCs).

UT7/Epo-S1 cells: UT7/Epo-S1 cells, a human megakaryoblastoid cell line obtained from Dr. Kevin Brown with permission from Dr. Kazuo Sugamura (89), were cultured under normoxic conditions in Dulbecco's modified Eagle's medium containing 10% fetal bovine serum and erythropoietin (2 U/ml; Amgen, Thousand Oaks, CA).

Virus and infection.

Plasma sample #404 that contains B19V at 1×10^{12} viral genomic copies per ml (vgc/ml) as quantified by qPCR was provided by ViraCor Eurofins Laboratories (Lee's Summit, MO). CD36$^+$ EPCs were infected with B19V at a multiplicity of infection (MOI) of 1,000 vgc per cell. After 2 days under hypoxia incubation, the infected cells were collected for flow cytometry and extraction of low-molecular weight (Hirt) DNA (41). In addition, at 18 h, 30 h, and 48 h post-infection, total DNA was extracted from cells for qPCR.

Electroporation.

Two million of UT7/Epo-S1 cells were electroporated with 3 μg of Sal I-linearized B19V infectious clone pM20 (48) in Solution V using Amaxa Nucleofector (Lonza, Basel, Switzerland), as described previously (29). After electroporation, the cells were cultured under hypoxia (1% O_2 and 5% CO_2) for two days.

Southern blot analysis.

Hirt DNA was extracted from either B19V-infected $CD36^+$ EPCs or B19V duplex genome (M20)-transfected UT7/Epo-S1 cells and was analyzed by Southern blotting as described previously (41). M20 excised from Sal I-digested pM20 was used as a probe. The blots were reprobed for mitochondrial (mt) DNA using a specific probe (90)

Protein expression and purification.

NS1 N terminal aa 1-176 (NS1N) and NS1N endonuclease motif mutant ($NS1N^{mEndo}$) coding sequences were ligated into vector pET-30a (GE Health Life Science) through Nde I and Xho I sites. Both plasmids were transformed into BL21(DE3)pLyss competent cells. Protein expression was induced by addition of IPTG in the bacterial culture at 1 mM. Protein was purified with a Ni-NTA affinity agarose (QIAGEN) as described previously (42).

***In vitro* DNA nicking assays.**

Radioactive nicking assay: Oligonucleotide (oligo) was 5' end-labeled with and [γ-^{32}P]ATP (PerkinElmer, Inc.) using T4 polynucleotide kinase (NEB). The labelled oligo was purified using MicroSpin G-50 columns (GE Healthcare). ^{32}P-labeled oligo and NS1N at final concentrations of 2 nM and 2 μM, respectively, were added in the nicking buffer (50 mM HEPES-NaOH, pH 7.0, 150 mM NaCl, and 10 mM $CoCl_2$) in a total volume of 20 μL. The reaction was incubated at 37°C for 16-18 h, and was quenched by the addition of 20 μL of quenching solution (80% formamide, 50 mM EDTA, 1 mg/mL xylene cyanol FF dye, and 1

mg/mL bromophenol blue dye), before electrophoresis on denaturing polyacrylamide [20% acrylamide:bis (acrylamide) (19:1 ratio), 4 M urea, 89 mM Tris base, 89 mM boric acid, and 2 mM EDTA] gels. The gels were autoradiographed without drying against a phosphor screen at 4°C for 12−18 h. Images were obtained by scanning the phosphor screen on a GE Typhoon FLA 9000 scanner (GE Healthcare) and processed with ImageQuant TL (GE Healthcare) software for quantification.

Fluorophore-based nicking assay: Fluorescein (FAM) labeled oligos were synthesized with 6-carboxyfluorescein (6-FAM) at the 5' end and Iowa Black® FQ quencher at the 3' end at Integrated DNA Technologies, Inc. (Coralville, Iowa). The labeled oligo was diluted to 100 µM as a stock solution. The *in vitro* nicking reaction was set up at 60 µL, which was composed of labelled oligo at 200 nM and purified NS1N at 2 µM in the nicking buffer. After incubation for 16-18 h, the samples were transferred to a black 96-well plate (Corning, cat. #3991). The fluorescence intensity of each sample was detected with excitation at 492 nm and emission at 518 nm on a microplate reader (Synergy H1 BioTek).

IC_{50}, EC_{50}, and CC_{50} determinations.

Half maximal inhibitory concentration (IC_{50}): In the fluorophore-based nicking assay, various concentrations of each inhibitor were used in the *in vitro* nicking reaction with Ori20 oligo. Fluorescence intensity of reactions with $^{FAM}Ori20^{Q}$ but without NS1N were set up as background. Fluorescence readings of the reactions with each concentration of the compound were compared with the DMSO (1%) control. The IC_{50} of each compound was calculated using GraphPad Prism.

Half maximal effective concentration (EC_{50}) based on viral capsid expression: This is the concentration at which half of the virus replication is inhibited in cells. For UT7/Epo-S1 cells, the cells were cultured under hypoxic conditions for 2 days, and then the cells were transfected with B19V duplex genome M20. Transfected cells were diluted with medium to 0.4

440 million/ml and transferred 1 ml to 12-well plates, followed by addition of a compound at various
441 concentrations. After 2 days under hypoxic conditions, the cells were collected for flow
442 cytometry to detect the capsid-expressing cells. For $CD36^+$ EPCs, compounds were added to
443 B19V-infected $CD36^+$ EPCs at various concentrations. After 2 days, the infected cells were
444 collected for flow cytometry to detect the capsid positive cells. The final EC_{50} was calculated
445 using GraphPad Prism. DMSO (0.1%) was used as a vehicle control.

446 **EC_{50} determined based on levels of viral DNA:** Day 6 $CD36^+$ EPCs were cultured
447 under hypoxic condition for 2 days, then the cells were infected with B19V for 1 h and washed
448 three times with the culture medium. The infected cells were diluted with the medium to 0.4
449 million/ml, of which cells of 0.1 ml were transferred to wells of a 96-well plate, followed by
450 addition of compounds at various concentrations. At 18 h, 30 h and 48 h post-infection,
451 infected cells were collected for extraction of total DNA using the DNeasy Blood&Tissue Kit
452 (Qiagen) following manufacturer's instructions. A multiplex qPCR assay using a set of probe
453 and primers targeting the B19V VP1 unique region-coding sequence and a set of probe and
454 primers targeting cellular mitochondrial DNA was used to quantify the viral DNA and cellular
455 DNA, respectively. The final EC_{50} was calculated using GraphPad Prism with the ratio of B19V
456 DNA/mt DNA related to the DMSO (0.1%) control group.

457 **Drug concentration that affects viability of 50% of cells in culture (CC_{50}):** UT7/Epo-
458 S1 cells or Day 6 $CD36^+$ EPCs were cultured under hypoxic condition for 2 days, and then the
459 cells were diluted with medium to 0.4 million/ml and transferred 0.1 ml to 96-well plates.
460 Compounds were added with different concentrations. After 2 days, the cell viability was
461 determined using CytoTox-Glo™ Cytotoxicity Assay kit (Promega) followed manufacturer's
462 instructions. We used GraphPad Prism to calculate the CC_{50}.

463

464 **Flow cytometry.**

465 To determine B19V capsid-expressing cells, infected or transfected cells were collected,
466 fixed and permeabilized as described previously (29). A mouse anti-B19V capsid monoclonal
467 antibody (clone 521-5D; MilliporeSigma, cat no.: MAB8292) was used to detect capsid-
468 expressing cells on a 3-laser flow cytometer (LSR II; BD Biosciences, San Jose, CA). All flow
469 data were analyzed using FACS DIVA software (BD Biosciences).
470
471 **Quantification of viral and mt DNA using multiplex qPCR.**
472 The primers and FAM-labelled probe for quantification of B19V DNA are VP1u forward
473 primer (5'-CCT GGG CAA GTT AGC GTA C-3'; nt 2975-2993), VP1u reverse primer (5'-ATG
474 AAT CCT TGC AGC ACT GTC A-3'; nt 3082-3061), and the VP1u probe (5'-/6-FAM/CCG GTA
475 CTA/ZEN/ACT ATG TTG GGC CTG GCA A/3IABkFQ/-3'; nt 3000-3027). The primers and JOE-
476 labelled probe for quantification of mt DNA are the mt forward primer (5'-TCA AAC TCA AAC
477 TAC GCC CTG-3'; nt 3673-3693), the mt reverse primer (5'-GTT GTG ATA AGG GTG GAG
478 AGG-3'; nt 3809-3789), and the mt probe (5'/6-JOEN/TGC GAG CAG/ZEN/TAG CCC AAA CAA
479 TCT/3IABkFQ/-3'; nt 3704-3727). Multiple PCR was performed as described previously (41,49)
480 on the 7500 Real-Time Fast PCR System (Applied Biosystems). Nucleotide sequences of B19V
481 and mitochondrial DNA refer to GenBank accessions AY386330.1 and GU170821.1,
482 respectively.
483
484 **Statistical analyses.**
485 GraphPad Prism8 software was used to calculate IC_{50}, EC_{50} and CC_{50} using inhibitor vs.
486 response-variable slope (four parameters).
487 For the correlation (r value) between data of two methods (the two assays) was
488 analyzed by Pearson Correlation using SPSS software (IBM Corp, Armonk, NY). When
489 comparing two methods through SPSS analysis, the coefficient of correlation was $p < 0.01$,

which was considered to be significant. The two methods are considered to be highly correlated as long as $r \geqslant 0.8$. Scatter plot, trendline and R^2 were calculated at the same time.

ACKNOWLEDGMENTS

We would like to thank members in the Qiu and Tavis labs for technical support and valuable discussions. We acknowledge the Flow Cytometry Core Laboratory, The University of Kansas Medical Center, for help in flow cytometry analysis. We also would like to thank Sarah McNitt and Max Bourdillon for the synthesis of compounds. This study was supported by PHS grant R01 AI070723 (to JQ), R01 AI104494 (to JET), and R21 AI124672 (to JET&MJM) from the National Institute of Allergy and Infectious Diseases. The funders had no role in study design, data collection and interpretation, or the decision to submit the work for publication.

REFERENCES

1. **Cossart, Y. E., A. M. Field, B. Cant, and D. Widdows**. 1975. Parvovirus-like particles in human sera. Lancet. **1**:72-73.

2. **Cotmore, S. F., M. Agbandje-McKenna, J. A. Chiorini, D. V. Mukha, D. J. Pintel, J. Qiu, M. Söderlund-Venermo, P. Tattersall, P. Tijssen, D. Gatherer, and A. J. Davison**. 2014. The family Parvoviridae. Arch.Virol. **159**:1239-1247.

3. **Ozawa, K., G. Kurtzman, and N. Young**. 1986. Replication of the B19 parvovirus in human bone marrow cell cultures. Science. **233**:883-886.

4. **Srivastava, A. and L. Lu**. 1988. Replication of B19 parvovirus in highly enriched hematopoietic progenitor cells from normal human bone marrow. J.Virol. **62**:3059-3063.

5. **Yaegashi, N., T. Niinuma, H. Chisaka, S. Uehara, S. Moffatt, K. Tada, M. Iwabuchi, Y. Matsunaga, M. Nakayama, C. Yutani, Y. Osamura, E. Hirayama, K. Okamura, K. Sugamura, and A. Yajima**. 1999. Parvovirus B19 infection induces apoptosis of erythroid cells in vitro and in vivo. J.Infect. **39**:68-76.

6. **Morey, A. L. and K. A. Fleming**. 1992. Immunophenotyping of fetal haemopoietic cells permissive for human parvovirus B19 replication in vitro. Br.J.Haematol. **82**:302-309.

7. **Anderson, M. J., M. N. Khousam, D. J. Maxwell, S. J. Gould, L. C. Happerfield, and W. J. Smith**. 1988. Human parvovirus B19 and hydrops fetalis. Lancet. **1**:535.

8. **Nunoue, T., K. Okochi, P. P. Mortimer, and B. J. Cohen**. 1985. Human parvovirus (B19) and erythema infectiosum. J.Pediatr. **107**:38-40.

9. **Chorba, T., P. Coccia, R. C. Holman, P. Tattersall, L. J. Anderson, J. Sudman, N. S. Young, E. Kurczynski, U. M. Saarinen, and R. Moir**. 1986. The role of parvovirus B19 in aplastic crisis and erythema infectiosum (fifth disease). J.Infect.Dis. **154**:383-393.

10. **Qiu, J., M. Söderlund-Venermo, and N. S. Young**. 2017. Human parvoviruses . Clin.Microbiol.Rev. **30**:43-113.

11. **Young, N. S. and K. E. Brown**. 2004. Parvovirus B19. N.Engl.J.Med. **350**:586-597.

12. **de Jong, E. P., T. R. de Haan, A. C. Kroes, M. F. Beersma, D. Oepkes, and F. J. Walther**. 2006. Parvovirus B19 infection in pregnancy. J.Clin.Virol. **36**:1-7.

13. **Woolf, A. D., G. V. Campion, A. Chishick, S. Wise, B. J. Cohen, P. T. Klouda, O. Caul, and P. A. Dieppe**. 1989. Clinical manifestations of human parvovirus B19 in adults. Arch.Intern.Med. **149**:1153-1156.

14. **Al-Khan, A., A. Caligiuri, and J. Apuzzio**. 2003. Parvovirus B-19 infection during pregnancy. Infect.Dis.Obstet.Gynecol. **11**:175-179.

15. **Chisaka, H., E. Morita, N. Yaegashi, and K. Sugamura**. 2003. Parvovirus B19 and the pathogenesis of anaemia. Rev.Med.Virol. **13**:347-359.

16. **Sol, N., J. J. Le, I. Vassias, J. M. Freyssinier, A. Thomas, A. F. Prigent, B. B. Rudkin, S. Fichelson, and F. Morinet**. 1999. Possible interactions between the NS-1 protein and tumor necrosis factor alpha pathways in erythroid cell apoptosis induced by human parvovirus B19. J.Virol. **73**:8762-8770.

17. **Morita, E. and K. Sugamura**. 2002. Human parvovirus B19-induced cell cycle arrest and apoptosis. Springer Semin.Immunopathol. **24**:187-199.

18. **Chen, A. Y., E. Y. Zhang, W. Guan, F. Cheng, S. Kleiboeker, T. M. Yankee, and J. Qiu**. 2010. The small 11kDa non-structural protein of human parvovirus B19 plays a key role in inducing apoptosis during B19 virus infection of primary erythroid progenitor cells. Blood. **115**:1070-1080.

19. **Moffatt, S., N. Yaegashi, K. Tada, N. Tanaka, and K. Sugamura**. 1998. Human parvovirus B19 nonstructural (NS1) protein induces apoptosis in erythroid lineage cells. J.Virol. **72**:3018-3028.

20. **Lou, S., Y. Luo, F. Cheng, Q. Huang, W. Shen, S. Kleiboeker, J. F. Tisdale, Z. Liu, and J. Qiu**. 2012. Human Parvovirus B19 DNA Replication Induces a DNA Damage Response That is Dispensable for Cell Cycle Arrest at G2/M Phase. J.Virol. **86**:10748-10758.

21. **Brown, K. E. and N. Young**. 1997. Human parvovirus B19: Pathogenesis of disease, p. 105-119. *In*: L. J. Anderson and N. Young (eds.), Human parvovirus B19., vol. 20. Karger, Basel, Switzerland.

22. **Chen, A. Y. and J. Qiu**. 2010. Parvovirus infection-induced cell death and cell cycle arrest. Future Virology **5**:731-741.

23. **Liu, Z., J. Qiu, F. Cheng, Y. Chu, Y. Yoto, M. G. O'Sullivan, K. E. Brown, and D. J. Pintel**. 2004. Comparison of the transcription profile of simian parvovirus with that of the human erythrovirus B19 reveals a number of unique features. J.Virol. **78**:12929-12939.

24. **Cotmore, S. F., V. C. McKie, L. J. Anderson, C. R. Astell, and P. Tattersall**. 1986. Identification of the major structural and nonstructural proteins encoded by human parvovirus B19 and mapping of their genes by procaryotic expression of isolated genomic fragments. J.Virol. **60**:548-557.

25. **Ganaie, S. S. and J. Qiu**. 2018. Recent Advances in Replication and Infection of Human Parvovirus B19. Front Cell Infect.Microbiol. **8**:166.

26. **Wan, Z., N. Zhi, S. Wong, K. Keyvanfar, D. Liu, N. Raghavachari, P. J. Munson, S. Su, D. Malide, S. Kajigaya, and N. S. Young**. 2010. Human parvovirus B19 causes cell cycle arrest of human erythroid progenitors via deregulation of the E2F family of transcription factors. J.Clin.Invest. **120**:3530-3544.

27. **Tewary, S. K., H. Zhao, X. Deng, J. Qiu, and L. Tang**. 2014. The human parvovirus B19 non-structural protein 1 N-terminal domain specifically binds to the origin of replication in the viral DNA. Virology. **449**:297-303.

28. **Sanchez, J. L., Z. Romero, A. Quinones, K. R. Torgeson, and N. C. Horton**. 2016. DNA Binding and Cleavage by the Human Parvovirus B19 NS1 Nuclease Domain. Biochemistry. **55**:6577-6593.

29. **Xu, P., Z. Zhou, M. Xiong, W. Zou, X. Deng, S. S. Ganaie, S. Kleiboeker, J. Peng, K. Liu, S. Wang, S. Q. Ye, and J. Qiu**. 2017. Parvovirus B19 NS1 protein induces cell cycle arrest at G2-phase by activating the ATR-CDC25C-CDK1 pathway. PLoS.Pathog. **13**:e1006266.

30. **Zhi, N., I. P. Mills, J. Lu, S. Wong, C. Filippone, and K. E. Brown**. 2006. Molecular and functional analyses of a human parvovirus B19 infectious clone demonstrates essential roles for NS1, VP1, and the 11-kilodalton protein in virus replication and infectivity. J.Virol. **80**:5941-5950.

31. **Gareus, R., A. Gigler, A. Hemauer, M. Leruez-Ville, F. Morinet, H. Wolf, and S. Modrow**. 1998. Characterization of cis-acting and NS1 protein-responsive elements in the p6 promoter of parvovirus B19. J.Virol. **72**:609-616.

32. **Moffatt, S., N. Tanaka, K. Tada, M. Nose, M. Nakamura, O. Muraoka, T. Hirano, and K. Sugamura**. 1996. A cytotoxic nonstructural protein, NS1, of human parvovirus B19 induces activation of interleukin-6 gene expression. J.Virol. **70**:8485-8491.

33. **Nakashima, A., E. Morita, S. Saito, and K. Sugamura**. 2004. Human Parvovirus B19 nonstructural protein transactivates the p21/WAF1 through Sp1. Virology. **329**:493-504.

34. **Cotmore, S. F. and P. Tattersall**. 2014. Parvoviruses: Small Does Not Mean Simple. Annu.Rev.Virol **1**:517-537.

35. **Weitzman, M. D. and R. M. Linden**. 2011. Adeno-associated virus biology. Methods Mol.Biol. **807**:1-23.

36. **Wang, Z., X. Deng, W. Zou, J. F. Engelhardt, Z. Yan, and J. Qiu**. 2017. Human Bocavirus 1 Is a Novel Helper for Adeno-Associated Virus Replication. J.Virol. **91**:e00710-17.

37. **Luo, Y., S. Lou, X. Deng, Z. Liu, Y. Li, S. Kleiboeker, and J. Qiu**. 2011. Parvovirus B19 infection of human primary erythroid progenitor cells triggers ATR-Chk1 signaling, which promotes B19 virus replication. J.Virol. **85**:8046-8055.

38. **Luo, Y., S. Kleiboeker, X. Deng, and J. Qiu**. 2013. Human parvovirus B19 infection causes cell cycle arrest of human erythroid progenitors at late S phase that favors viral DNA replication. J.Virol. **87**:12766-12775.

39. **Luo, Y. and J. Qiu**. 2015. Human parvovirus B19: a mechanistic overview of infection and DNA replication. Future Virol. **10**:155-167.

40. **Zou, W., Z. Wang, M. Xiong, A. Y. Chen, P. Xu, S. S. Ganaie, Y. Badawi, S. Kleiboeker, H. Nishimune, S. Q. Ye, and J. Qiu**. 2018. Human Parvovirus B19 Utilizes Cellular DNA Replication Machinery for Viral DNA Replication. J.Virol. **92**:e01881-17.

41. **Guan, W., S. Wong, N. Zhi, and J. Qiu**. 2009. The genome of human parvovirus B19 virus can replicate in non-permissive cells with the help of adenovirus genes and produces infectious virus. J.Virol. **83**:9541-9553.

42. **Ganaie, S. S., W. Zou, P. Xu, X. Deng, S. Kleiboeker, and J. Qiu**. 2017. Phosphorylated STAT5 directly facilitates parvovirus B19 DNA replication in human erythroid progenitors through interaction with the MCM complex. PLoS.Pathog. **13**:e1006370.

43. **Cai, C. W., E. Lomonosova, E. A. Moran, X. Cheng, K. B. Patel, F. Bailly, P. Cotelle, M. J. Meyers, and J. E. Tavis**. 2014. Hepatitis B virus replication is blocked by a 2-hydroxyisoquinoline-1,3(2H,4H)-dione (HID) inhibitor of the viral ribonuclease H activity. Antiviral Res. **108**:48-55.

44. **Tavis, J. E., X. Cheng, Y. Hu, M. Totten, F. Cao, E. Michailidis, R. Aurora, M. J. Meyers, E. J. Jacobsen, M. A. Parniak, and S. G. Sarafianos**. 2013. The hepatitis B virus ribonuclease H is sensitive to inhibitors of the human immunodeficiency virus ribonuclease H and integrase enzymes. PLoS.Pathog. **9**:e1003125.

45. **Tavis, J. E. and E. Lomonosova**. 2015. The hepatitis B virus ribonuclease H as a drug target. Antiviral Res. **118**:132-138.

46. **Lomonosova, E., J. Daw, A. K. Garimallaprabhakaran, N. B. Agyemang, Y. Ashani, R. P. Murelli, and J. E. Tavis**. 2017. Efficacy and cytotoxicity in cell culture of novel alpha-hydroxytropolone inhibitors of hepatitis B virus ribonuclease H. Antiviral Res. **144**:164-172.

47. **Edwards, T. C., E. Lomonosova, J. A. Patel, Q. Li, J. A. Villa, A. K. Gupta, L. A. Morrison, F. Bailly, P. Cotelle, E. Giannakopoulou, G. Zoidis, and J. E. Tavis**. 2017.

635 Inhibition of hepatitis B virus replication by N-hydroxyisoquinolinediones and related
636 polyoxygenated heterocycles. Antiviral Res. **143**:205-217.

637 48. **Zhi, N., Z. Zadori, K. E. Brown, and P. Tijssen**. 2004. Construction and sequencing of
638 an infectious clone of the human parvovirus B19. Virology **318**:142-152.

639 49. **Chen, A. Y., S. Kleiboeker, and J. Qiu**. 2011. Productive Parvovirus B19 Infection of
640 Primary Human Erythroid Progenitor Cells at Hypoxia is Regulated by STAT5A and MEK
641 Signaling but not HIF alpha. PLoS.Pathog. **7**:e1002088.

642 50. **Kurtzman, G., N. Frickhofen, J. Kimball, D. W. Jenkins, A. W. Nienhuis, and N. S.**
643 **Young**. 1989. Pure red-cell aplasia of 10 years' duration due to persistent parvovirus
644 B19 infection and its cure with immunoglobulin therapy. N.Engl.J.Med. **321**:519-523.

645 51. **Mouthon, L., L. Guillevin, and Z. Tellier**. 2005. Intravenous immunoglobulins in
646 autoimmune- or parvovirus B19-mediated pure red-cell aplasia. Autoimmun.Rev. **4**:264-
647 269.

648 52. **Young, N. S.** 1996. Parvovirus infection and its treatment. Clin.Exp.Immunol. **104 Suppl**
649 **1**:26-30.

650 53. **Hayakawa, F., K. Imada, M. Towatari, and H. Saito**. 2002. Life-threatening human
651 parvovirus B19 infection transmitted by intravenous immune globulin. Br.J.Haematol.
652 **118**:1187-1189.

653 54. **Egbuna, O., M. S. Zand, A. Arbini, M. Menegus, and J. Taylor**. 2006. A cluster of
654 parvovirus B19 infections in renal transplant recipients: a prospective case series and
655 review of the literature. Am.J.Transplant. **6**:225-231.

656 55. **Renoult, E., C. Bachelet, M. J. Krier-Coudert, A. Diarrassouba, J. L. Andre, and M.**
657 **Kessler**. 2006. Recurrent anemia in kidney transplant recipients with parvovirus B19
658 infection. Transplant.Proc. **38**:2321-2323.

659 56. **Ogawa, E., S. Otaguro, M. Murata, M. Kainuma, Y. Sawayama, N. Furusyo, and J.**
660 **Hayashi**. 2008. Intravenous immunoglobulin therapy for severe arthritis associated with
661 human parvovirus B19 infection. J.Infect.Chemother. **14**:377-382.

662 57. **Shen, Q., H. Xu, Q. Cao, L. J. Zhou, J. Xu, X. Y. Fang, and J. Ge**. 2011. Long-term
663 remission of recurrent severe anemia as a result of parvovirus B19 infection in a
664 pediatric renal transplant recipient. Pediatr.Transplant. **15**:E76-E79.

665 58. **Mrzljak, A., I. Kardum-Skelin, V. C. Cvrlje, T. F. Kanizaj, D. Sustercic, D. Gustin,**
666 **and B. Kocman**. 2010. Parvovirus B 19 (PVB19) induced pure red cell aplasia (PRCA)
667 in immunocompromised patient after liver transplantation. Coll.Antropol. **34**:271-274.

668 59. **Moudgil, A., H. Shidban, C. C. Nast, A. Bagga, S. Aswad, S. L. Graham, R. Mendez,**
669 **and S. C. Jordan**. 1997. Parvovirus B19 infection-related complications in renal
670 transplant recipients: treatment with intravenous immunoglobulin. Transplantation.
671 **64**:1847-1850.

60. **Koduri, P. R., R. Kumapley, N. D. Khokha, and A. R. Patel**. 1997. Red cell aplasia caused by parvovirus B19 in AIDS: use of i.v. immunoglobulin. Ann.Hematol. **75**:67-68.

61. **Ramratnam, B., A. Gollerkeri, F. J. Schiffman, P. Rintels, and T. P. Flanigan**. 1995. Management of persistent B19 parvovirus infection in AIDS. Br.J.Haematol. **91**:90-92.

62. **Koduri, P. R., R. Kumapley, J. Valladares, and C. Teter**. 1999. Chronic pure red cell aplasia caused by parvovirus B19 in AIDS: use of intravenous immunoglobulin--a report of eight patients. Am.J.Hematol. **61**:16-20.

63. **Hung, C. C., K. L. Lee, and M. Y. Chen**. 2001. Increase in B19 viral load prior to relapse of anaemia in an AIDS patient with persistent B19 infection. J.Infect. **43**:150-152.

64. **Bonvicini, F., G. Bua, E. Manaresi, and G. Gallinella**. 2015. Antiviral effect of cidofovir on parvovirus B19 replication. Antiviral Res. **113**:11-18.

65. **Bonvicini, F., G. Bua, E. Manaresi, and G. Gallinella**. 2016. Enhanced inhibition of parvovirus B19 replication by cidofovir in extendedly exposed erythroid progenitor cells. Virus Res. **220**:47-51.

66. **Cushnie, T. P. and A. J. Lamb**. 2005. Antimicrobial activity of flavonoids. Int.J.Antimicrob.Agents. **26**:343-356.

67. **Mansuri, M. L., P. Parihar, I. Solanki, and M. S. Parihar**. 2014. Flavonoids in modulation of cell survival signalling pathways. Genes Nutr. **9**:400-0400.

68. **Zakaryan, H., E. Arabyan, A. Oo, and K. Zandi**. 2017. Flavonoids: promising natural compounds against viral infections. Arch.Virol. **162**:2539-2551.

69. **Hung, P. Y., B. C. Ho, S. Y. Lee, S. Y. Chang, C. L. Kao, S. S. Lee, and C. N. Lee**. 2015. Houttuynia cordata targets the beginning stage of herpes simplex virus infection. PLoS.ONE. **10**:e0115475.

70. **Argenta, D. F., I. T. Silva, V. L. Bassani, L. S. Koester, H. F. Teixeira, and C. M. Simoes**. 2015. Antiherpes evaluation of soybean isoflavonoids. Arch.Virol. **160**:2335-2342.

71. **Qian, K., A. J. Gao, M. Y. Zhu, H. X. Shao, W. J. Jin, J. Q. Ye, and A. J. Qin**. 2014. Genistein inhibits the replication of avian leucosis virus subgroup J in DF-1 cells. Virus Res. **192**:114-120.

72. **Ganesan, S., A. N. Faris, A. T. Comstock, Q. Wang, S. Nanua, M. B. Hershenson, and U. S. Sajjan**. 2012. Quercetin inhibits rhinovirus replication in vitro and in vivo. Antiviral Res. **94**:258-271.

73. **Min, N., P. T. Leong, R. C. H. Lee, J. S. E. Khuan, and J. J. H. Chu**. 2018. A flavonoid compound library screen revealed potent antiviral activity of plant-derived flavonoids on human enterovirus A71 replication. Antiviral Res. **150**:60-68.

74. **Lin, Y. J., Y. C. Chang, N. W. Hsiao, J. L. Hsieh, C. Y. Wang, S. H. Kung, F. J. Tsai, Y. C. Lan, and C. W. Lin**. 2012. Fisetin and rutin as 3C protease inhibitors of enterovirus A71. J.Virol.Methods. **182**:93-98.

75. **Yang, L., J. Lin, B. Zhou, Y. Liu, and B. Zhu**. 2017. Activity of compounds from Taxillus sutchuenensis as inhibitors of HCV NS3 serine protease. Nat.Prod.Res. **31**:487-491.

76. **Bachmetov, L., M. Gal-Tanamy, A. Shapira, M. Vorobeychik, T. Giterman-Galam, P. Sathiyamoorthy, A. Golan-Goldhirsh, I. Benhar, R. Tur-Kaspa, and R. Zemel**. 2012. Suppression of hepatitis C virus by the flavonoid quercetin is mediated by inhibition of NS3 protease activity. J.Viral Hepat. **19**:e81-e88.

77. **Yu, M. S., J. Lee, J. M. Lee, Y. Kim, Y. W. Chin, J. G. Jee, Y. S. Keum, and Y. J. Jeong**. 2012. Identification of myricetin and scutellarein as novel chemical inhibitors of the SARS coronavirus helicase, nsP13. Bioorg.Med Chem.Lett. **22**:4049-4054.

78. **Behbahani, M., S. Sayedipour, A. Pourazar, and M. Shanehsazzadeh**. 2014. In vitro anti-HIV-1 activities of kaempferol and kaempferol-7-O-glucoside isolated from Securigera securidaca. Res Pharm.Sci. **9**:463-469.

79. **Nakane, H. and K. Ono**. 1989. Differential inhibition of HIV-reverse transcriptase and various DNA and RNA polymerases by some catechin derivatives. Nucleic Acids Symp.Ser.115-116.

80. **Wang, C., P. Wang, X. Chen, W. Wang, and Y. Jin**. 2015. Saururus chinensis (Lour.) Baill blocks enterovirus 71 infection by hijacking MEK1-ERK signaling pathway. Antiviral Res. **119**:47-56.

81. **Cotmore, S. F. and P. Tattersall**. 2005. A rolling-haipin strategy: basic mechanisms of DNA replication in the parvoviruses, p. 171-181. *In*: J. Kerr, S. F. Cotmore, M. E. Bloom, R. M. Linden, and C. R. Parrish (eds.), Parvoviruses. Hoddler Arond, London.

82. **Lu, G., J. A. Villa, M. J. Donlin, T. C. Edwards, X. Cheng, R. F. Heier, M. J. Meyers, and J. E. Tavis**. 2016. Hepatitis B virus genetic diversity has minimal impact on sensitivity of the viral ribonuclease H to inhibitors. Antiviral Res. **135**:24-30.

83. **Meck, C., M. P. D'Erasmo, D. R. Hirsch, and R. P. Murelli**. 2014. The biology and synthesis of alpha-hydroxytropolones. Medchemcomm. **5**:842-852.

84. **Su, H. P., Y. Yan, G. S. Prasad, R. F. Smith, C. L. Daniels, P. D. Abeywickrema, J. C. Reid, H. M. Loughran, M. Kornienko, S. Sharma, J. A. Grobler, B. Xu, V. Sardana, T. J. Allison, P. D. Williams, P. L. Darke, D. J. Hazuda, and S. Munshi**. 2010. Structural basis for the inhibition of RNase H activity of HIV-1 reverse transcriptase by RNase H active site-directed inhibitors. J.Virol. **84**:7625-7633.

85. **Summa, V., A. Petrocchi, F. Bonelli, B. Crescenzi, M. Donghi, M. Ferrara, F. Fiore, C. Gardelli, P. O. Gonzalez, D. J. Hazuda, P. Jones, O. Kinzel, R. Laufer, E. Monteagudo, E. Muraglia, E. Nizi, F. Orvieto, P. Pace, G. Pescatore, R. Scarpelli, K. Stillmock, M. V. Witmer, and M. Rowley**. 2008. Discovery of raltegravir, a potent,

selective orally bioavailable HIV-integrase inhibitor for the treatment of HIV-AIDS infection. J Med Chem. **51**:5843-5855.

86. **Masaoka, T., H. Zhao, D. R. Hirsch, M. P. D'Erasmo, C. Meck, B. Varnado, A. Gupta, M. J. Meyers, J. Baines, J. A. Beutler, R. P. Murelli, L. Tang, and S. F. Le Grice**. 2016. Characterization of the C-Terminal Nuclease Domain of Herpes Simplex Virus pUL15 as a Target of Nucleotidyltransferase Inhibitors. Biochemistry. **55**:809-819.

87. **Williams, P. D., S. Venkatraman, H. M. Langford, B. Kim, T. M. Booth, J. A. Grobler, D. Staas, R. D. Ruzek, M. W. Embrey, C. M. Wiscount, and T. A. Lyle**. 2007. 1-hydroxy naphthyridine compounds as anti-hiv agents. US patent PCT/US2007/016052.

88. **Wong, S., N. Zhi, C. Filippone, K. Keyvanfar, S. Kajigaya, K. E. Brown, and N. S. Young**. 2008. Ex vivo-generated CD36+ erythroid progenitors are highly permissive to human parvovirus B19 replication. J.Virol. **82**:2470-2476.

89. **Morita, E., A. Nakashima, H. Asao, H. Sato, and K. Sugamura**. 2003. Human parvovirus B19 nonstructural protein (NS1) induces cell cycle arrest at G(1) phase. J.Virol. **77**:2915-2921.

90. **Sowd, G. A., N. Y. Li, and E. Fanning**. 2013. ATM and ATR activities maintain replication fork integrity during SV40 chromatin replication. PLoS.Pathog. **9**:e1003283.

91. **Deng, X., Z. Yan, F. Cheng, J. F. Engelhardt, and J. Qiu**. 2016. Replication of an Autonomous Human Parvovirus in Non-dividing Human Airway Epithelium Is Facilitated through the DNA Damage and Repair Pathways. PLoS.Pathog. **12**:e1005399.

FIGURE LEGENDS

Fig. 1. Functional domains of B19V NS1 and purification of NS1N and NS1N^{mEndo} proteins.

(A) A schematic diagram of the B19V NS1 protein. The B19V NS1 is depicted with the Ori-binding (OBD/Endonuclease), Helicase, and Transactivation domains. NS1N has the NS1 aa 1-176, and NS1N^{mEndo} has alanine substitutions in the endonuclease motif (aa 140-143) (20). The Walker boxes, NTP-binding sites, and the zinc finger motifs are indicated. The C-terminal region (shown in yellow) contains a transactivation domain 2 (TAD2) (^{523}SSFFNLITP^{531}) (20). **(B&C) Purification of NS1N and NS1N^{mEndo} proteins.** One liter of IPTG-induced bacteria was collected, sonicated, and lysed. The cleared lysate was mixed with ~1 ml NTA beads (Qiagen) and loaded onto a column. The beads were then washed with Wash buffer, followed

by elution buffer. Each fraction was collected at ~1ml, and 20 µl was loaded for SDS-15%-PAGE. The gels were stained with Coomassie blue. Dialyzed fraction F2 or F3 was used in the *in vitro* nicking assay.

Fig. 2. Purified B19V NS1N specifically cleaves the B19V ssDNA Ori at the terminal resolution site.

(A) The sequences of Ori30, Ori30^{mut} and a size marker of 19-nt (M19). The core sequence of the Ori is shown with the STAT5BE, terminal resolution site (trs), and NS1-binding elements (NS1BEs). The Ori30 probe and the Ori30^{mut} probe that has three mutations (in blue) at the trs site are shown. The nicked DNA fragments from the Ori30 are shown under the arrowhead. **(B-C) Radioactive *in vitro* nicking assay.** Reactions of *in vitro* nicking were analyzed on denaturing polyacrylamide gel, together with labeled probes alone and a labeled oligo of 19-nt as a size marker of the cleaved band. (B) NS1N cleaved Ori30 but not Ori30^{mut}. ^{32}P-labeled Ori30 or Ori30^{mut} was incubated with NS1N in the nicking buffer. (C) NS1N, but not NS1N^{mEndo}, cleaved Ori30. ^{32}P-labeled Ori30 was incubated with NS1N or NS1N^{mEndo} in the nicking buffer. **(D) Determination of a minimal concentration of NS1N used in the nicking reactions.** 2 nM ^{32}P-labeled Ori30 oligo was incubated with NS1N at a final concentration of 0.1, 0.5, 2 and 4 µM, respectively, in the nicking buffer.

Fig. 3. Compound screening for inhibition of cleavage of the ^{32}P-labeled B19V Ori30 oligo.

A total of 96 small molecule compounds at 100 µM (A) or the chosen 25 compounds at 10 µM (B) were incubated with ^{32}P-labeled Ori30 and NS1N in the nicking buffer. The reactions were analyzed on denaturing polyacrylamide gel. Relative nicking efficiencies are shown. The ratio of the signals at 19-nt vs. 19-nt plus 30-nt in the DMSO vehicle control group is set up 1. **(A)** Compounds inhibited all nicking activity are shown in blank as no obvious nicked bands at 19-nt

were detected. **(B)** Autoradiography gel images for the 25 compounds assessed at 10 μM are shown.

Fig. 4. Establishment of a 6-carboxyfluorescein (FAM)-based *in vitro* nicking assay.

(A) A diagram of the FAM-labeled oligos. Sequences of the Ori20 is shown with FAM and Iowa Black® FQ quencher (Q) at 5' and 3' ends, respectively. After incubation with NS1N, Ori20 is cleaved into two shorter oligos, and then FAM-linked short oligo of 9-nt is released for fluorescence detection. **(B) ^{FAM}Ori20^{Q}-based nicking assay.** 200 nM ^{FAM}Ori20^{Q} were incubated with 2 μM NS1N protein in the nicking buffer. The fluorescence intensity of each sample was detected on a microplate reader. ^{FAM}Ori20^{Q} without NS1N, and ^{FAM}Ori20 without a quencher were used as controls. **(C) Optimization of the probe concentration.** Various concentrations of the ^{FAM}Ori20^{Q} probe were used in the nicking assay. Fluorescence intensity was determined with or without NS1N as indicated. The fold changes in the presence of NS1N compared with no NS1N are shown.

Fig. 5. Screening of compounds for inhibition of cleavage of the B19V Ori by NS1N using FAM-labeled B19V Ori20.

(A) FAM-based *in vitro* nicking assay. Each of the 71 compounds were incubated with NS1N at 10 μM in the nicking buffer at 37°C for 16-18 h. The fluorescence intensity of each sample was detected on a microplate reader. Ori20 without NS1N was set up as background, and Ori20 with NS1N and DMSO was set up as positive control. We set up an inhibition of 80% of the relative fluorescence intensity as a cutoff value for the inhibition of NS1N nicking. **(B) Comparison of the 25 chosen compounds between the radioactive and fluorescent nicking assays.** At the final concentration of 10 μM, 8 compounds showed inhibition of >80% in the NS1N nicking of the ^{32}P-labeled Ori30 (in red), and 8 compounds showed positive in the NS1N nicking of the FAM-labeled Ori20 (in green). The correlation coefficient (r) between the

Antimicrobial Agents and Chemotherapy

radioactive and fluorescent nicking assays was calculated using SPSS software. **(C) Scatter plot and trendline of the radioactive nicking assay with the fluorescent nicking assay.** Scatter plot, trendline and R^2 of the two assays were calculated using SPSS software.

Fig. 6. Chemo structures of the eight screened compounds.

(A) Flavonoids. (B) Naphthyridinones.

Fig. 7. IC_{50} determination of compounds #7, #135 and #201.

In the FAM-based nicking assay, various concentrations of the compound were added to the nicking assay with $^{FAM}Ori20^{Q}$ and NS1N protein. The fluorescence intensity of each reaction was detected. $^{FAM}Ori20^{Q}$ without NS1N was set up as background. Each concentration was compared with DMSO. The IC_{50} of each inhibitor was calculated using GraphPad Prism.

Fig. 8. EC_{50} and CC_{50} determination of compounds #7, #135 and #201.

(A) EC_{50} determination. UT7/Epo-S1 cells were transfected with B19V duplex genome M20. Each inhibitor was added with different concentrations as labeled. After 2 days, the cells were collected for flow cytometry to detect the capsid-expressing cells. DMSO was used as a vehicle control. The final EC_{50} was calculated with GraphPad Prism. **(B) CC_{50} determination**. Compounds, at various concentration as shown, were added to UT7/Epo-S1 cells in 96-well plates. After 2 days, the percentage of viable cells were determined using CytoTox-Glo™ Cytotoxicity Assay kit (Promega), and the CC_{50} was calculated using GraphPad Prism.

Fig. 9. Compounds #7, #135 and #201 inhibit B19V DNA replication in UT7/Epo-S1 cells.

UT7/Epo-S1 cells were electroporated with B19V duplex genome M20, followed by addition of the compound #7 **(A)**, compound #135 **(B)**, or compound #201 **(C)** at various concentrations as shown. At two days post-transfection, Hirt DNA samples prepared from

856 treated cells were digested with Dpn I and subjected to Southern blotting with the M20 probe.
857 DMSO was used a vehicle control. UT7/Epo-S1 cells without transfection were set up as Mock.
858 pM20 digested with Sal I was loaded as size marker. Mitochondrial (mt) DNA was detected as
859 loading control using a specific mt DNA probe (91). *mRF DNA, monomer replicative form DNA,
860 and **ssDNA, single-strand DNA.
861
862 **Fig. 10. EC_{50} and CC_{50} determination of compound #7, compound #135 and compound**
863 **#201.**
864 **(A) EC_{50} determination**. $CD36^+$ EPCs were infected with B19V. Each compound was
865 added with different concentrations as shown. At 2 days post-infection, the cells were collected
866 for flow cytometry to detect the capsid-expressing cells. DMSO was used as a vehicle control.
867 The final EC_{50} was calculated with GraphPad Prism. **(B) CC_{50} determination.** EPCs in 96-well
868 plates were treated with each compound at various concentrations as shown. At 2 days post-
869 infection, percentages of viable cells were determined, and the CC_{50} was calculated using
870 GraphPad Prism.
871
872 **Fig. 11. Compounds #7, #135 and #201 inhibit B19V replication in $CD36^+$ EPCs.**
873 $CD36^+$ EPCs were infected with B19V followed by addition of each compound #7 **(A)**,
874 compound #135 **(B)** and compound #201**(C)** at various concentrations as shown. At two days
875 post-infection, Hirt DNA samples were prepared from infected cells, and were subjected to
876 Southern blotting using the M20 probe. DMSO was used a vehicle control. $CD36^+$ EPCs without
877 infection were set up as Mock. pM20 digest with Sal I was loaded as size marker. Mitochondrial
878 (mt) DNA was detected as loading control using a specific mt DNA probe (91). *mRF DNA,
879 monomer replicative form DNA, and **ssDNA, single-strand DNA.
880

881 **Fig. 12. Compounds #7, #135 and #201 inhibit B19V DNA replication in CD36$^+$ EPCs at 18**
882 **h, 30 h and 48 h post-infection.**

883 CD36$^+$ EPCs were infected with B19V followed by addition of Compound #7 **(A)**,
884 Compound #135 **(B)** and Compound #201 **(C)** at various concentrations as shown. At 18 h, 30 h,
885 48 h post-infection, total DNA was extracted from each sample and subjected to multiplex qPCR
886 for detection of viral DNA and cellular (mt) DNA. DMSO was used a vehicle control. The ratios
887 of B19V DNA/mt DNA were calculated and are shown related to the vehicle control (which is set
888 up 1). EC_{50} was calculated using GraphPad Prism.

Antimicrobial Agents and Chemotherapy

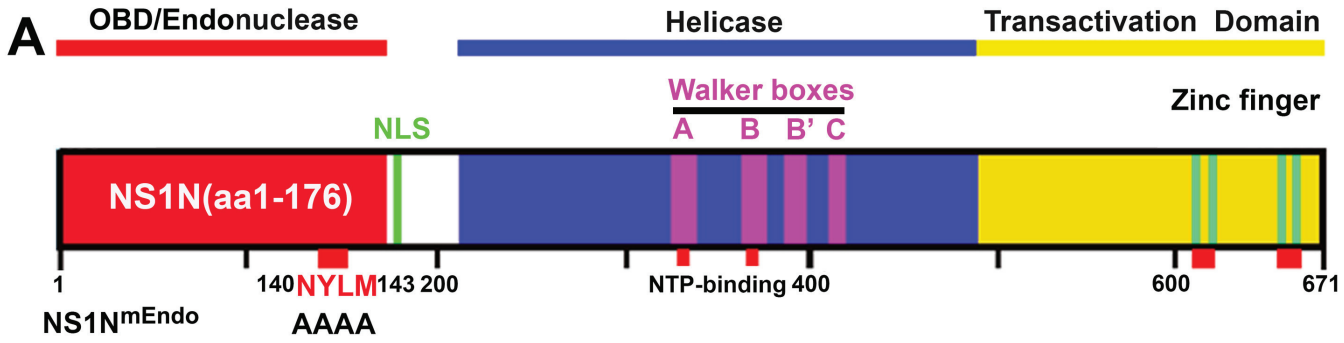

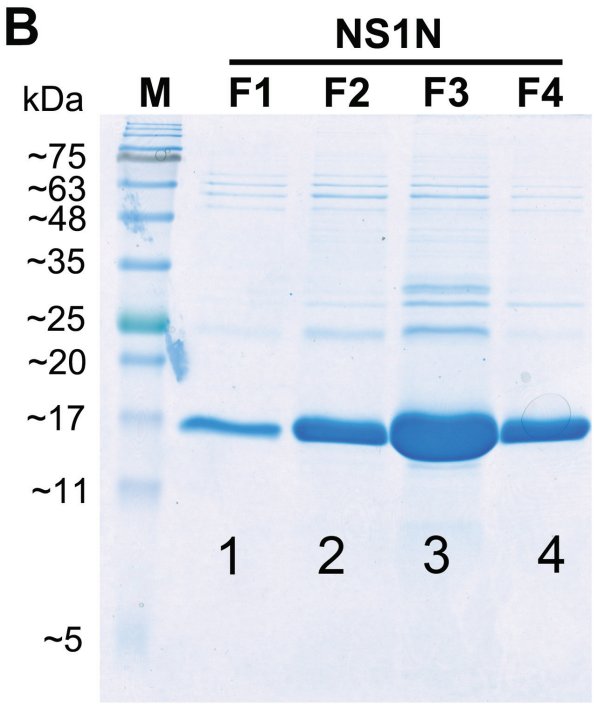

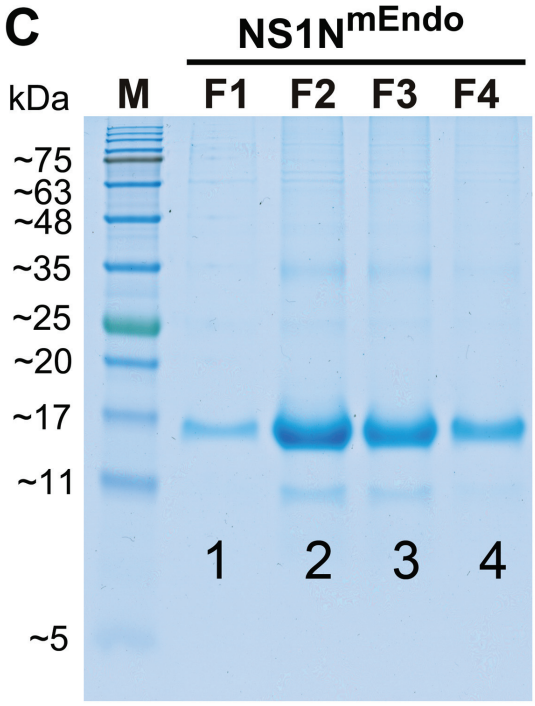

Figue 1

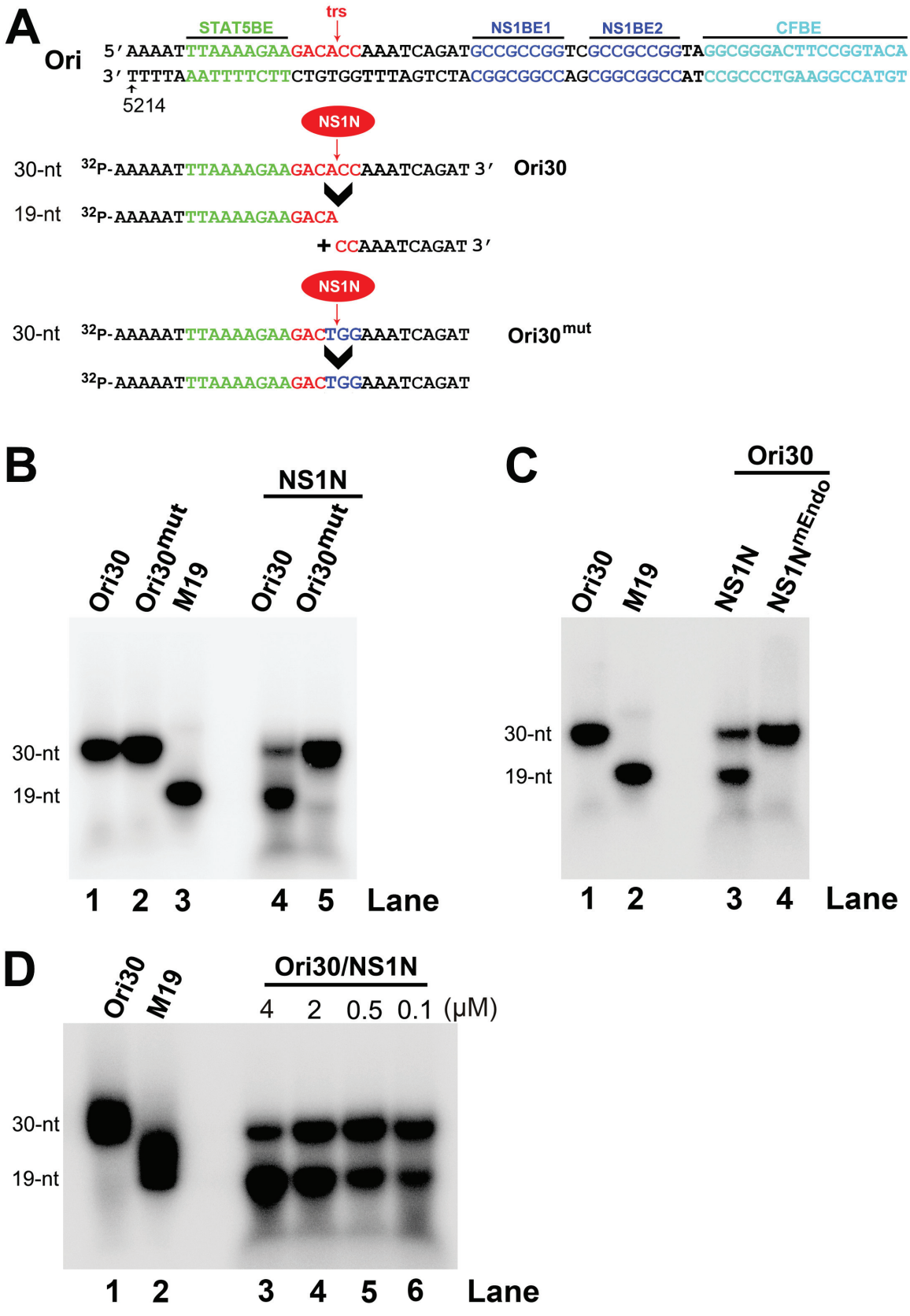

Figure 2

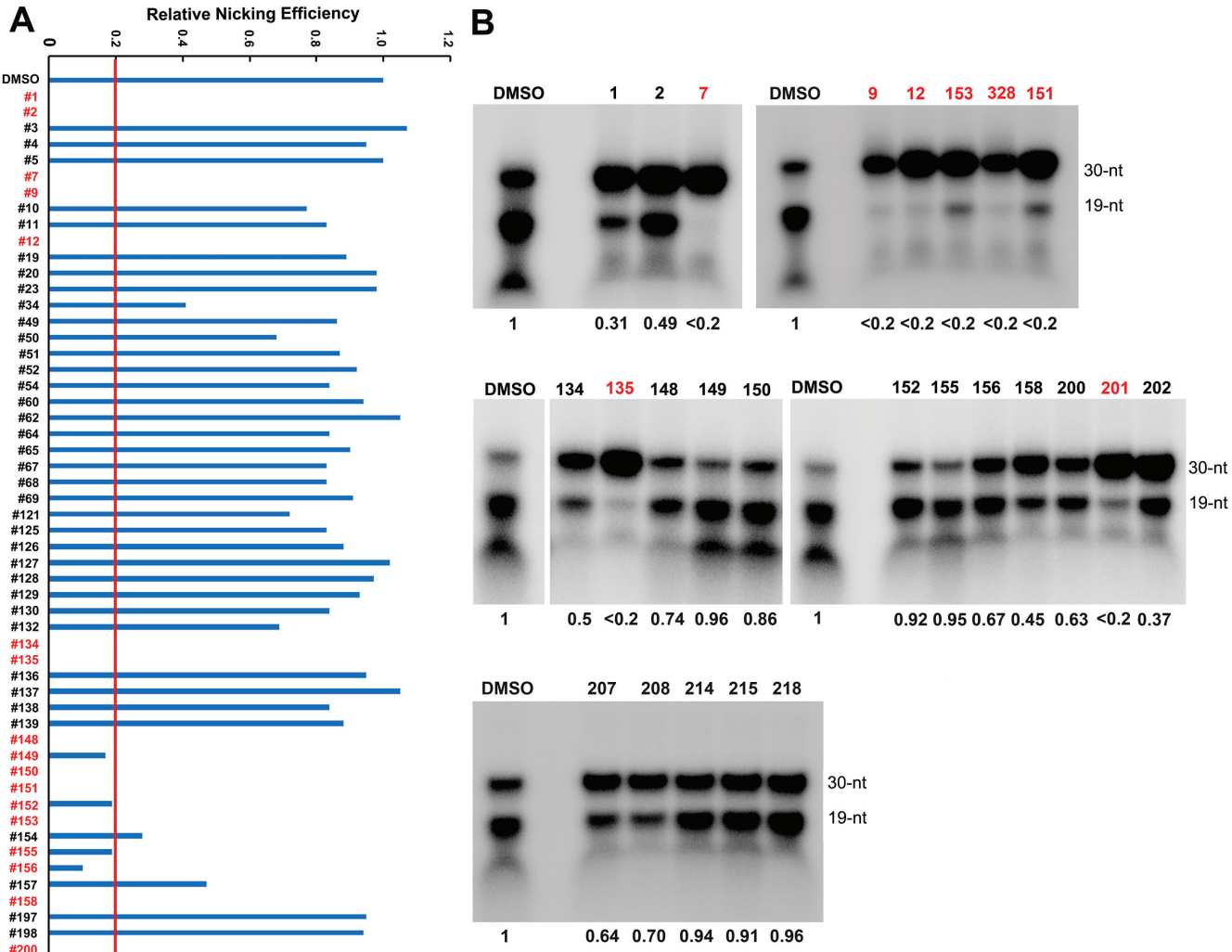

Figure 3

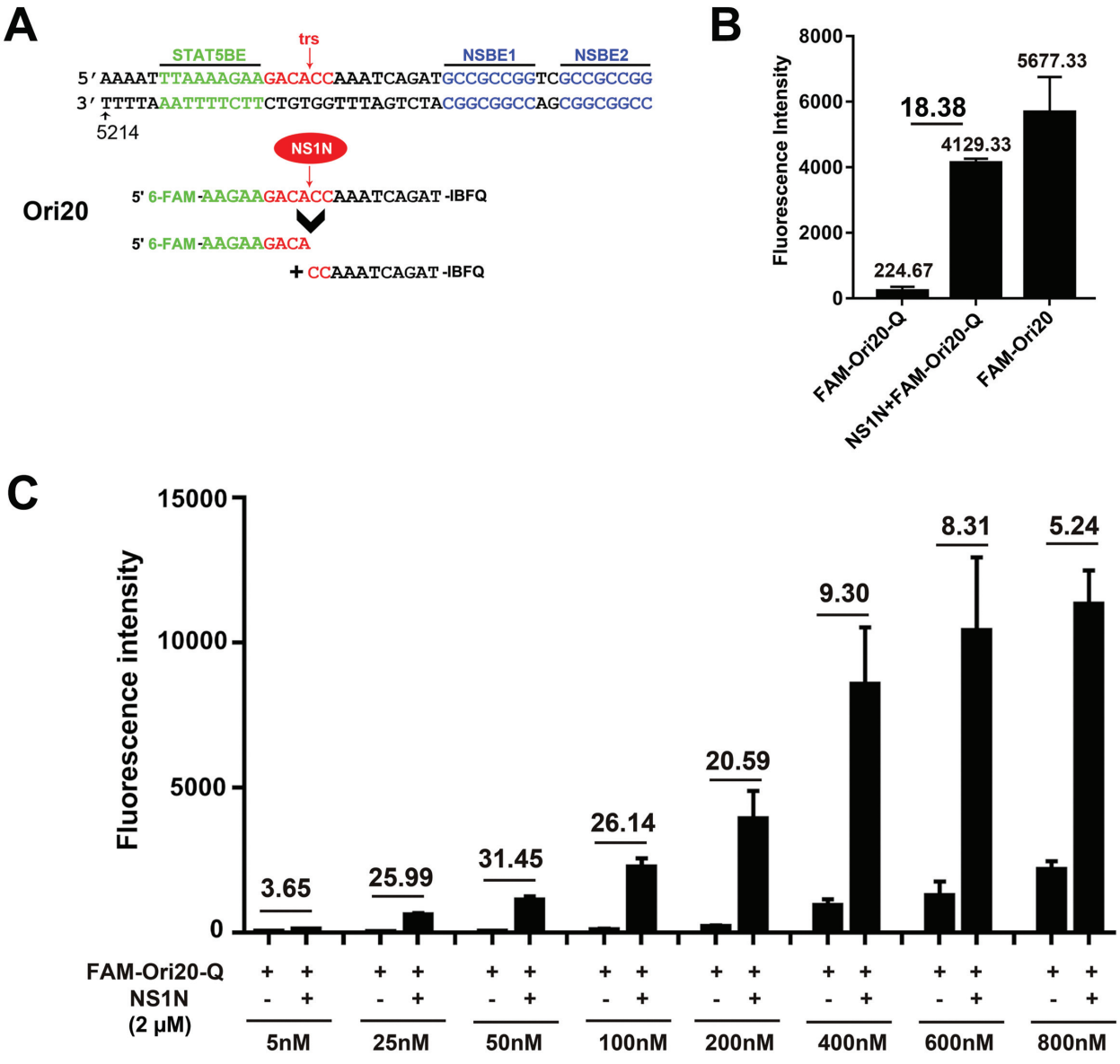

Figure 4

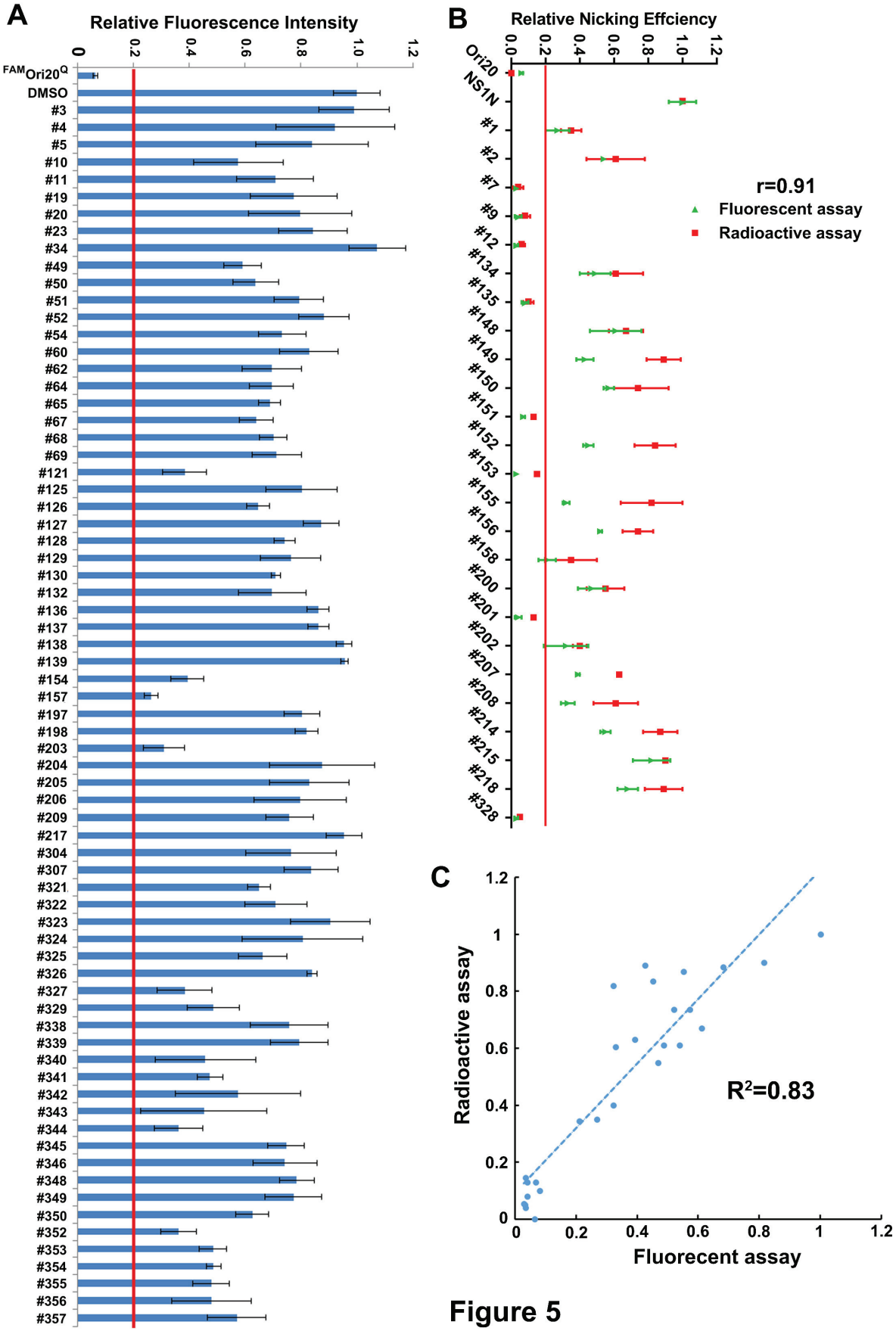

Figure 5

A **Flavonoid**

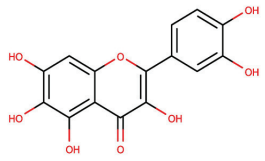

#7

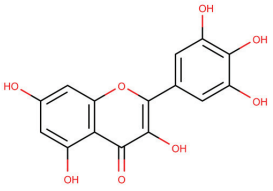

#9

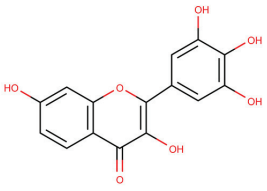

#135

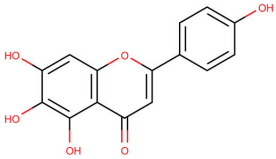

#201

B **Napthyridinone**

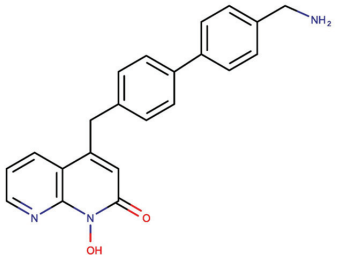

#12

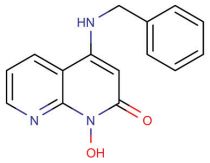

#151

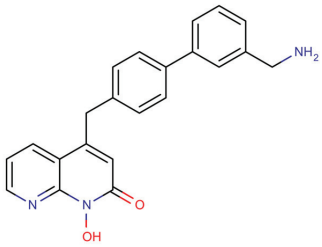

#153

Comparators:

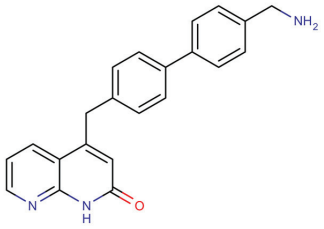

#150

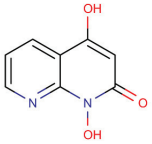

#148

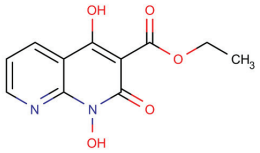

#152

Figure 6

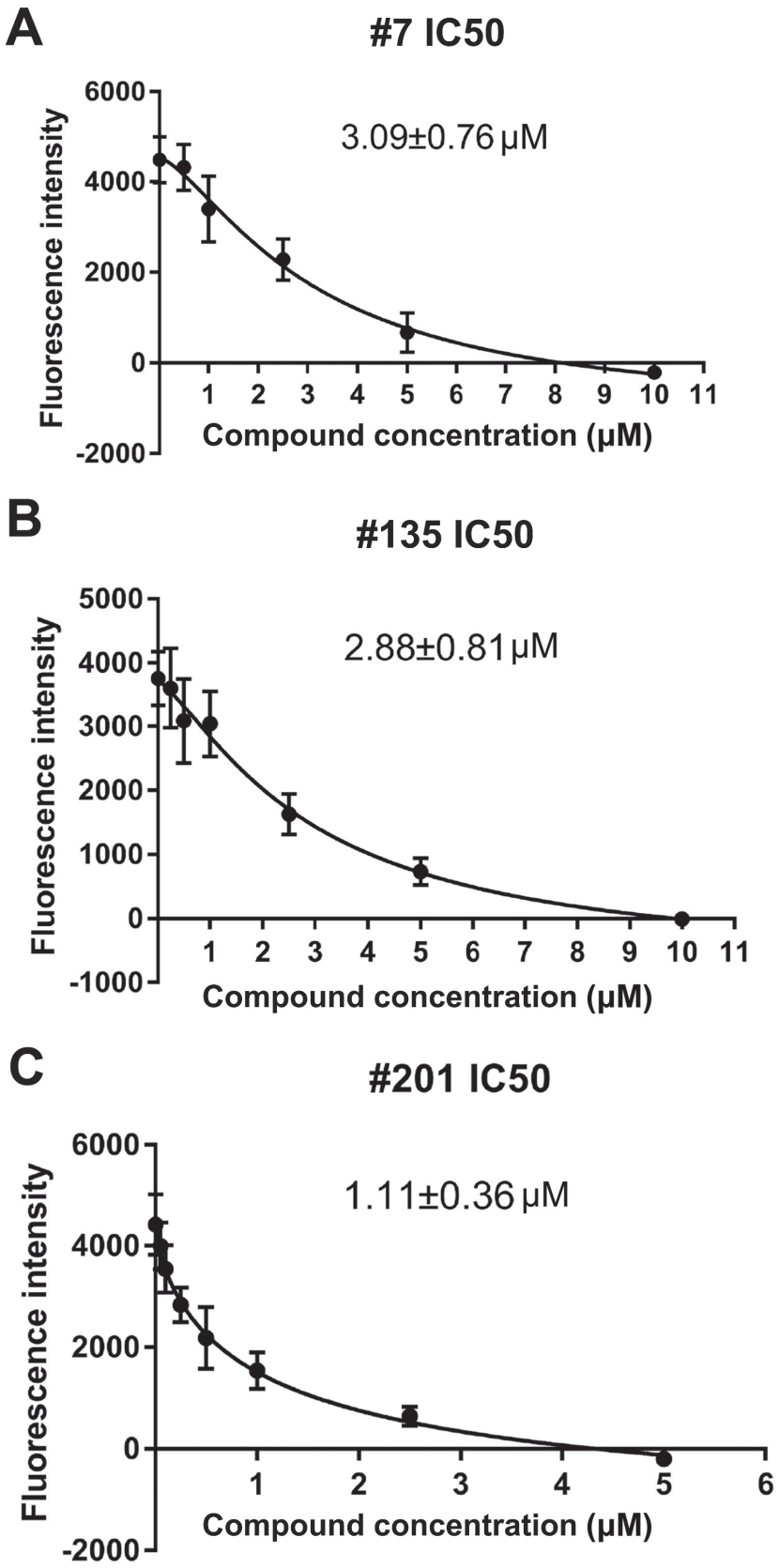

Figure 7

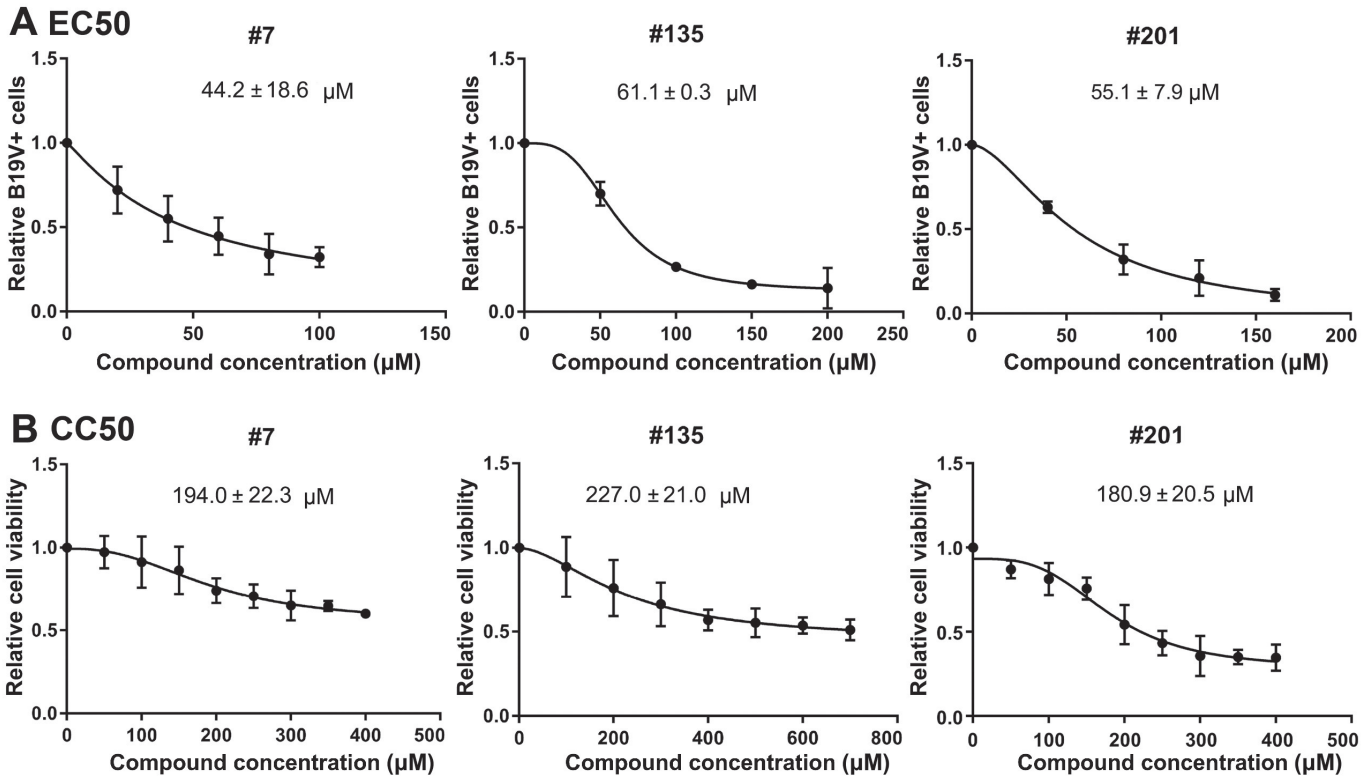

Figure 8

Antimicrobial Agents and Chemotherapy

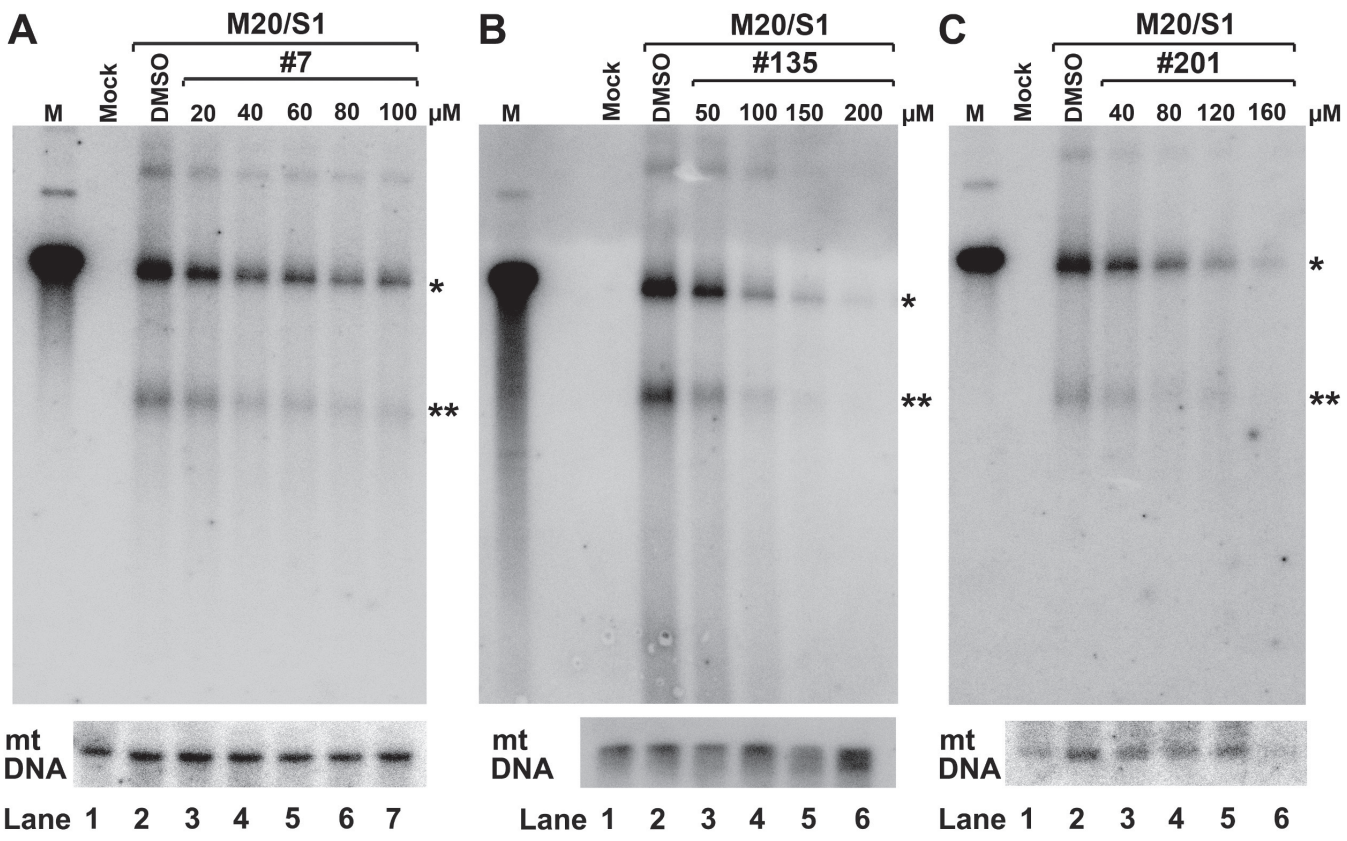

Figure 9

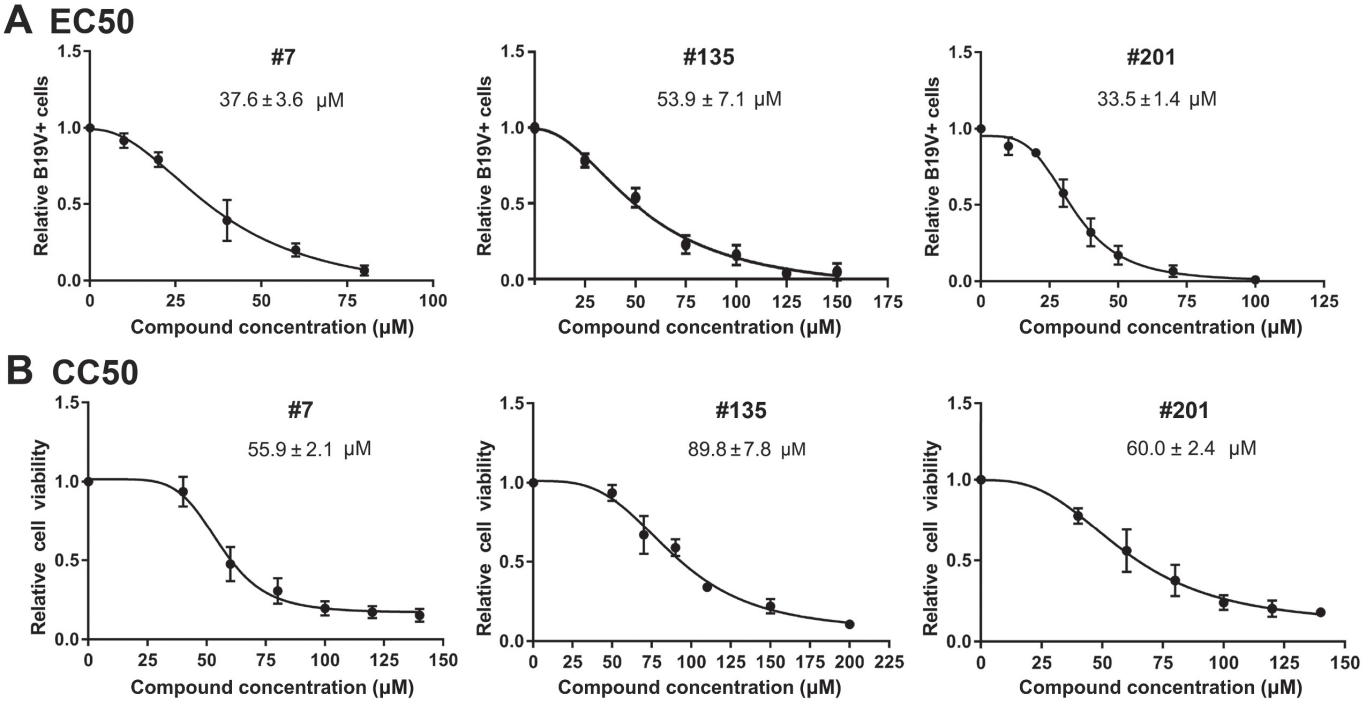

Figure 10

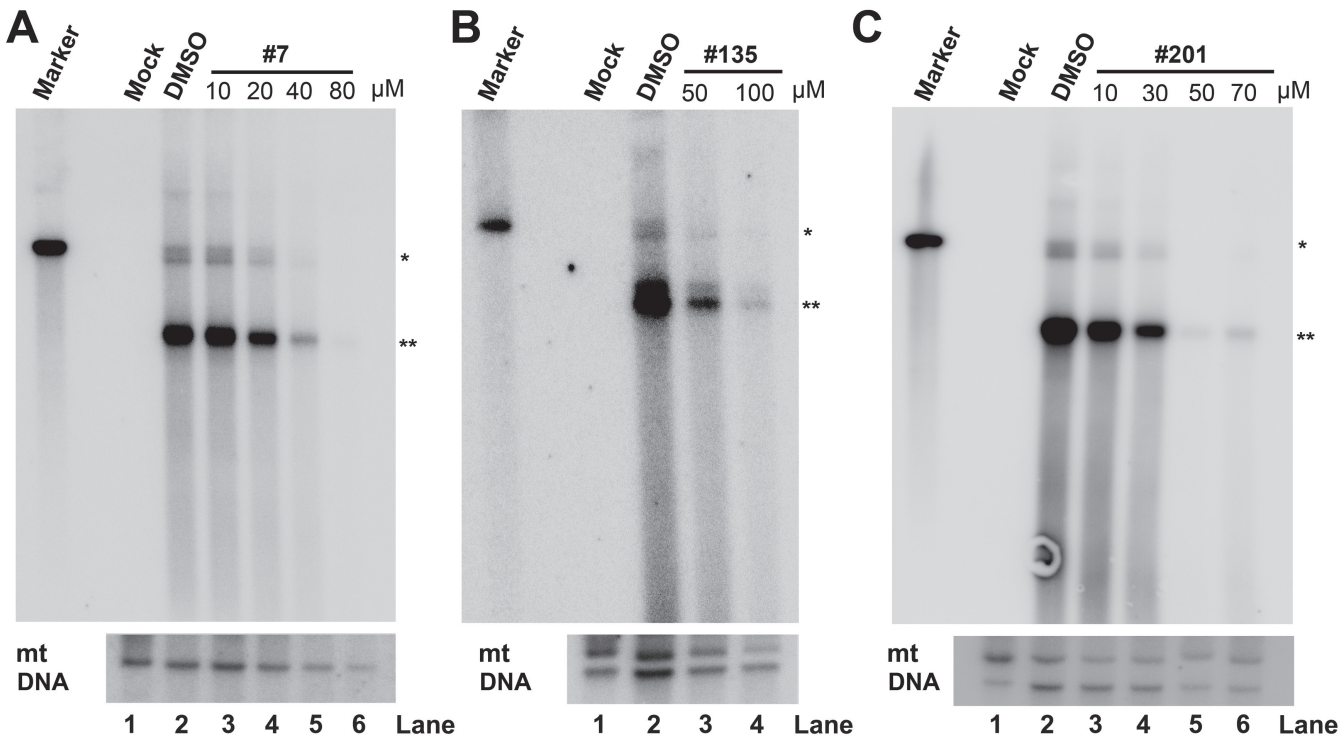

Figure 11

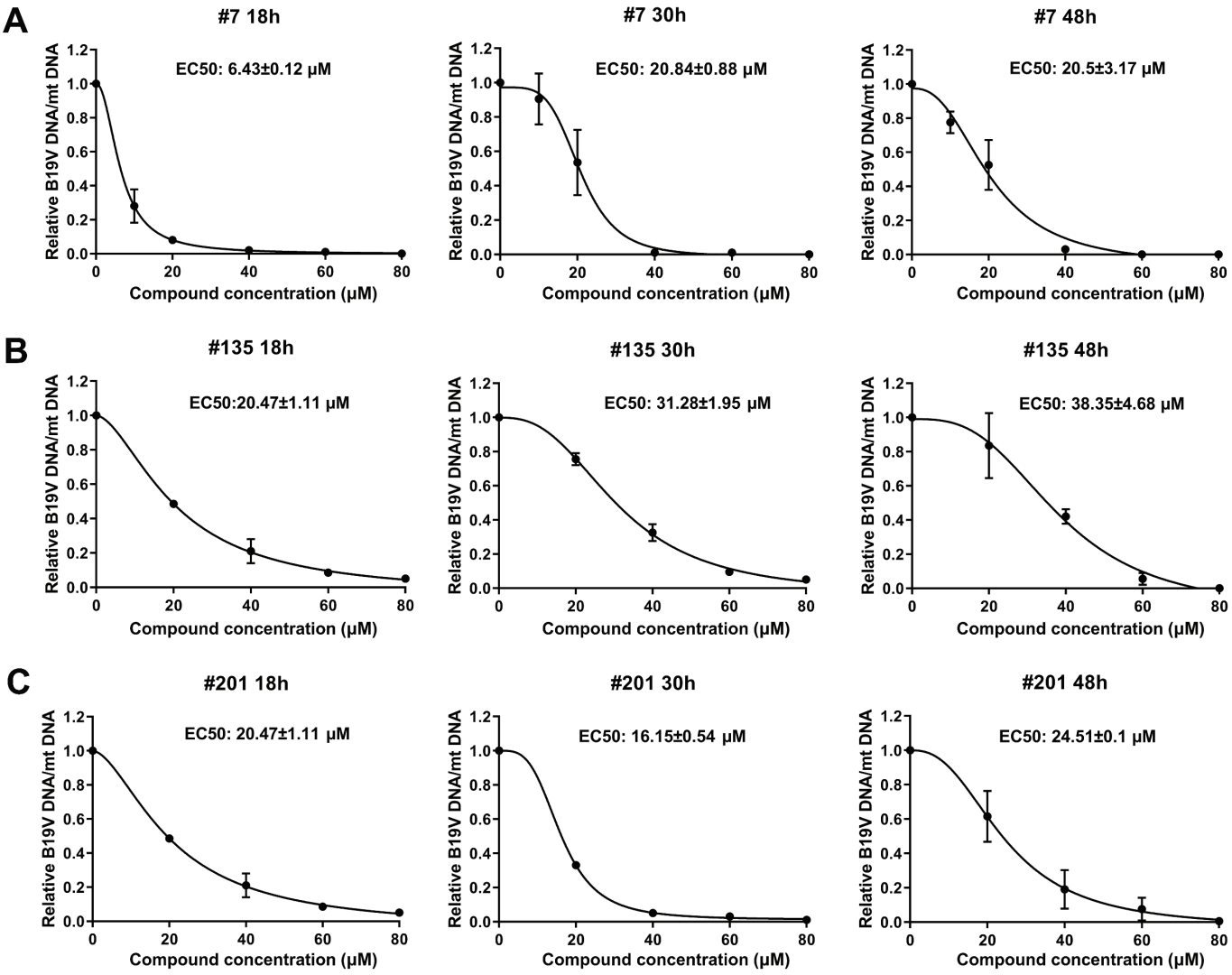

Figure 12

Antimicrobial Agents and Chemotherapy